Nanoscale Intermolecular Interactions between Human Serum Albumin and Low Grafting Density Surfaces of Poly(ethylene oxide)

M. A. Rixman,† D. Dean,‡ and C. Ortiz*,†

Department of Materials Science and Engineering and Department of Electrical Engineering and Computer Science, Massachusetts Institute of Technology, 77 Massachusetts Avenue, Cambridge, Massachusetts 02139

Received January 13, 2003. In Final Form: June 13, 2003

The net nanoscale interaction between a probe tip covalently bound with the blood plasma protein human serum albumin (HSA) and a surface of end-grafted poly(ethylene oxide) (PEO) mushrooms ($M_n \sim$ 50K, Flory radius $R_F \sim 9$ nm, contour length $L_{contour} \sim 393$ nm) was measured directly on approach (loading) and retract (unloading) in aqueous buffer solution using the technique of high-resolution force spectroscopy (HRFS). On approach of the HSA probe tip to the PEO surface, a monotonic nonlinear repulsive net force was observed for tip−sample separation distances of <30 nm, the magnitude of which is much larger than that predicted by either electrostatic double layer or steric theories based on configurational entropy. Attractive contacts between the PEO and HSA are formed during experimentation, enabling the tethering and extension of *individual* PEO chains on retraction. The mean binding force of the HSA probe tip to individual PEO chains was determined to be $\langle F_{adh} \rangle = 0.06 \pm 0.10$ nN or $\langle F_{adh}/\text{Radius} \rangle = 0.9 \pm 1.6$ mN/m (where Radius is the end radius of the probe tip as measured by scanning electron microscopy). By combining the results of HRFS experiments with theoretical approaches, we have shown that this technique is a valuable tool for understanding biocompatibility at the nanoscale and can provide valuable information that may be used as a guideline for the design of improved synthetic macromolecular systems for future biomedical applications.

Introduction

Approaches for improving the hemocompatibility of blood-contacting biomedical devices include the use of polymeric coatings in the form of physisorbed layers or end-grafted brushes,[1−3] self-assembling monolayers,[4−6] surface fixation of anticoagulants such as heparin, prostaglandin derivatives,[7] thrombolytic enzymes,[8] endothelial cell surface glycoproteins such as thrombomodulin,[9] polymers which exhibit the controlled release of nitric oxide (a potential platelet antiaggregating and vasodilating agent),[10] or endothelial cell seeding,[11] sometimes in conjunction with blood preclotting or precoating with fibronectin, laminin, albumin, collagen, gelatin, or RGD-containing peptides.[12−14] Poly(ethylene oxide) (PEO), poly(oxyethylene) (POE), or poly(ethylene glycol) (PEG), $-[CH_2-CH_2-O]_n-$, is a synthetic polymer that is typically thought of as biologically inert and is used extensively to provide a protective coating to improve the protein resistance of biomaterial surfaces. However, a variety of different experimental techniques have shown that proteins do indeed adsorb to PEO given enough time and certain disadvantageous conditions (e.g., high forces, dilute polymer solutions, long incubation times, etc.).[15−27] Despite extensive efforts and debates in the literature, the detailed molecular mechanism of the interaction of PEO with

* To whom correspondence should be addressed. Department of Materials Science and Engineering, RM 13-4022, 77 Massachusetts Avenue, Cambridge, MA 02139. E-mail: cortiz@mit.edu.

† Department of Materials Science and Engineering.

‡ Department of Electrical Engineering and Computer Science.

(1) Lee, J. H.; Lee, H. B.; Andrade, J. D. *Prog. Polym. Sci.* **1995**, *20*, 1043−1079.

(2) Leckband, D. *Annu. Rev. Biophys. Biomol. Struct.* **2000**, *29*, 1−26.

(3) Israelachvili, J. The different faces of poly(ethylene glycol). *Proc. Natl. Acad. Sci. U.S.A.* **1997**, *94*, 8378−8379.

(4) Ostuni, E.; Chapman, R. G.; Liang, M. N.; Meluleni, G.; Pier, G.; Ingber, D. E.; Whitesides, G. M. *Langmuir* **2001**, *17*, 6336−6343.

(5) Ostuni, E.; Holmlin, R. E.; Takayama, S.; Whitesides, G. M. *Langmuir* **2001**, *17*, 5605−5620.

(6) Holmlin, R. E.; Chen, X.; Chapman, R. G.; Takayama, S.; Whitesides, G. M. *Langmuir* **2001**, *17*, 2841−2850.

(7) Akashi, M.; Takeda, S.; Miyazaki, T.; Yashima, E.; Miyauchi, N. *J. Bioact. Compat. Polym.* **1989**, *4*, 4.

(8) Oshiro, T.; Kosaki, F. *Artif. Organs* **1980**, *4*, 58.

(9) Li, J.-M.; Singh, M. J.; Nelson, P. R.; Hendricks, G. M.; Itani, M.; Rohrer, M. J.; Cutler, B. S. *J. Surg. Res.* **2002**, *105*, 200−208.

(10) Mowery, K. A.; Schoenfischa, M. H.; Saavedrab, J. E.; Keeferc, L. K.; Meyerhoff, M. E. *Biomaterials* **2000**, *21*, 9−21.

(11) Pasic, M.; MullerGlauser, W. L. v.; Odermatt, B.; Lachat, M.; Turina, M. *J. Cardio-Thorac. Surg.* **1996**, *10*, 372−379.

(12) Sank, A.; Rostami, K.; Weaver, F.; Ertl, D.; Yellin, A.; Nimni, M.; Tuan, T. *Ann. J. Surg.* **1992**, *164*, 199.

(13) Thomson, G. J. L.; Vohra, R. K.; Carr, M. H.; Walker, M. G. *Surgery* **1990**, *109*, 20−27.

(14) Maroisa, Y.; Chakféa, N.; Guidoina, R.; Roya, R.; Maroisa, M.; Kinga, M. W.; Douvillea, Y. *Biomaterials* **1996**, *17*, 3−14.

(15) Abbott, N. L.; Blankschtein, D.; Hatton, T. A. *Macromolecules* **1992**, *25*, 3932−3941.

(16) Azegami, S.; Tsuboi, A.; Izumi, T.; Hirata, M.; Dubin, P. L.; Wang, B.; Kokufuta, E. *Langmuir* **1999**, *15*, 940−947.

(17) Sheth, S. R.; Leckband, D. Measurements of attractive forces between proteins and end-grafted poly(ethylene glycol) chains. *Proc. Natl. Acad. Sci. U.S.A.* **1997**, *94*, 8399−8404.

(18) Leckband, D.; Sheth, S.; Halperin, A. *J. Biomater. Sci., Polym. Ed.* **1999**, *10*, 1125−1147.

(19) Halperin, A.; Leckband, D. *C. R. Acad. Sci. Paris*: *Polymers at Interfaces* **2000**, *Series IV*, 1171−1178.

(20) Efremova, N. V.; Bondurant, B.; O'Brien, D. F.; Leckband, D. E. *Biochemistry* **2000**, *39*, 3441−3451.

(21) Xua, Z.; Marchant, R. E. *Biomaterials* **2000**, *21*, 1075−1083.

(22) Currie, E. P. K.; Van Der Gucht, J.; Borisov, O. V.; Stuart, M. A. C. *Pure Appl. Chem.* **1999**, *71*, 1227.

(23) Harris, J. M. In *Poly(ethylene glycol) Chemistry*: *Biotechnical and Biomedical Applications*; Plenum: New York, 1992.

(24) Efremova, N. V.; Huang, Y.; Peppas, N. A.; Leckband, D. E. *Langmuir* **2002**, *18*, 836−845.

(25) Cleland, J. L.; Builder, S. E.; Swartz, J. R.; Winkler, M.; Chang, J. Y.; Wang, D. I. C. *Bio/Technology* **1992**, *10*, 1013−1019.

(26) Furness, E.; Ross, A.; Davis, T. P.; King, G. C. *Biomaterials* **1998**, *19*, 1361−1369.

(27) Topchieva, I. N.; Efremova, N. V.; Khvorov, N. V.; Magretova, N. V. *Bioconjugate Chem.* **1995**, *6*, 380−388.

10.1021/la034057l CCC: $25.00
Published on Web 09/25/2003

proteins is still largely unknown. Following is a summary of the numerous suggested attractive and repulsive constituent contributions to the net protein−PEO intermolecular interaction potential as a function of separation distance, U(D).

PEO: Repulsive Interactions. PEO has a number of unique properties that are thought to be directly related to the presence of repulsive interactions which give it a distinctive capability for protein resistance. PEO is hydrophilic and generally water soluble at room temperature, with a relatively low Flory−Huggins interaction parameter ($\chi = 0.41-0.45$ at ~25 °C)[28] and high values of the second virial coefficient ($A_2 = 30-60 \times 10^4$ cm^3·mol/g^2 at ~25 °C[28]), due to its strong tendency to form hydrogen bonds with water via the −O− groups. The unique structure of PEO has been predicted by molecular dynamics simulations[29] and studied experimentally by infrared spectroscopy,[30,31] Raman spectroscopy,[32] nuclear magnetic resonance,[30,33] and single molecule force spectroscopy measurements[34] (all in aqueous solution), as well as calorimetry[35] and X-ray diffraction in the crystalline form.[36] It has been postulated that the majority of chain segments exist in a trans-trans-gauche (ttg) conformation that is stabilized by water binding, leading to an (11/2) helical supramolecular structure[35] that is similar to, but more expanded than, that found for the crystalline form (Figure 1A−C). As shown in Figure 1D, in the more extended planar trans-trans-trans (ttt) configuration, the distance between −O− atoms is large enough that a water molecule may only form one hydrogen bond with the PEO backbone. While it is known that the −O− atoms of PEO in the melt may chelate a variety of metal cations in the crystalline or melt form,[37] thus rendering a fixed positive charge along the chain, in *aqueous salt solution* PEO has been found experimentally in a number of reports to be incapable of chelating certain larger cations, including Na^+, K^+, NH_4^+, and CS^+.[38−41]

Since the buffer solution employed in all of our experiments presented in this paper has Na^+ and K^+ cations, the PEO is assumed to be effectively neutral; however, since mostly all proteins are typically charged under physiological conditions there is also the possibility of a repulsive electrostatic double layer force due to the local ionic osmotic pressure and Maxwell electric stress.[42] Correspondingly, attractive electrostatic interactions with proteins of net opposite charge or surface regions of a protein with opposite charge will be minimized. Since PEO does not have any bulky side groups or fixed charge groups, local steric and electrostatic hindrances are expected to be minimal (at 20 °C the steric parameter $\sigma = 1.38-2$ [28])

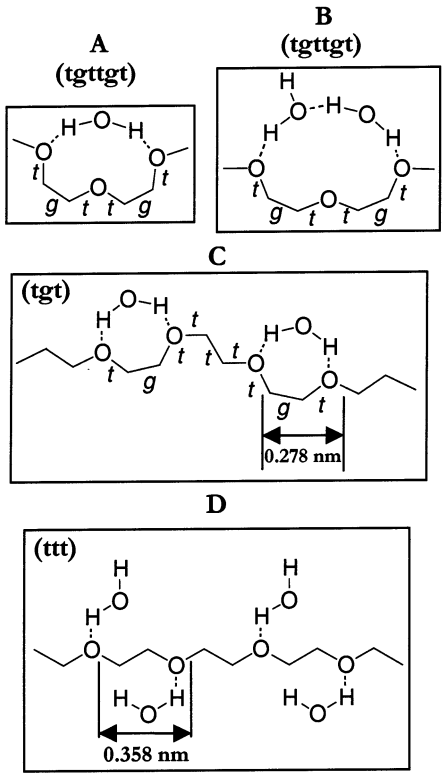

Figure 1. Possible conformations of PEO in aqueous solution: In water, PEO may take on a "folded" trans-trans-gauche (ttg) configuration in which the ether oxygen atoms undergo hydrogen bonding in a variety of different ways (A−C). The all-trans (ttt) planar zigzag conformation (D) is also shown.

and the chain's flexibility and mobility can help accommodate the shortened ttg conformation and continuous structural rearrangements with water. The strong affinity and binding with water thus create repulsive enthalpic penalties for disruption of these bonds and the helical supramolecular structure. Another repulsive force, which is not unique to PEO, arises from polymeric "steric" or "overlap" interactions, which are enhanced by long chains (i.e., high molecular weight) and high surface grafting densities. For end-grafted polymer brushes in a good solvent, there are two main components to the steric force that are determined: an attractive elastic restoring force due to configurational entropy and a repulsive osmotic pressure due to an increase in polymer chain segment concentration. The osmotic pressure originates from solvent translational entropy and intrachain excluded volume due to short-range monomer−solvent affinity and/or monomer−monomer repulsion. PEO has a large excluded volume due to its high affinity for water, as reflected by its low value of χ and high value of A_2. For compression of low-density surfaces of isolated, end-grafted polymer "mushrooms", the steric force arises from a free energy penalty for chain segment−surface confinement, as well as an entropic elastic penalty for chain stretching in the plane perpendicular to the compression axis.[43−46] Lastly, the compression of a polymer layer (e.g., by incoming proteins) will also be opposed by a hydrodynamic lubrication force due to lateral expulsion of the solvent residing between the protein and the surface.[47]

(28) Brandrup, J.; Immergut, E. H. In *Polymer Handbook*, 3rd ed.; Wiley: New York, 1989.
(29) Tasaki, K. *J. Am. Chem. Soc.* **1996**, *118*, 8459−8469.
(30) Matsura, H.; Miyazawa, T. *Bull. Chem. Soc. Jpn.* **1968**, *41*, 1798.
(31) Begum, R.; Matsuura, H. *J. Chem. Soc., Faraday Trans.* **1997**, *93*, 3839.
(32) Koenig, J. I.; Angood, A. C. *J. Polym. Sci.* **1970**, *8*, 1787−1796.
(33) Lui, K. J.; Parsons, J. L. *Macromolecules* **1969**, *2*, 529.
(34) Oesterhelt, F.; Rief, M.; Gaub, H. E. *New J. Phys.* **1999**, *1*, 6.1−6.11.
(35) Maron, S. H.; Filisko, F. E. *J. Macromol. Sci.* **1972**, *hys. B6*, 79.
(36) Tadokoro, H. *Structure of Crystalline Polymers*; Malabar: Kriege, 1990.
(37) London, J. D.; Annis, B. K.; Habenschuss, A.; Borodin, O.; Smith, G. D.; Turner, J. Z.; Soper, A. K. *Macromolecules* **1997**, *30*, 7151−7157.
(38) Armstrong, J. K.; Leharne, S. A.; Stuart, B. H.; Snowden, M. J.; Chowdhry, B. Z. *Langmuir* **2001**, *17*, 4482−4485.
(39) Scott, H. *J. Colloid Interface Sci.* **1973**, *43*.
(40) Irvine, D. J.; Mayes, A. M.; Satija, S. K.; Barker, S. J.; Sofia-Allgor, S. J.; Griffith, L. G. *J. Biomed. Mater. Res.* **1998**, *40*, 498−509.
(41) Schick, M. J. *J. Colloid Sci.* **1962**, *17*, 801−813.
(42) Sanfeld, A. *Thermodynamics of Charged and Polarized Layers*; Wiley-Interscience: Bath, U.K., 1968; Vol. 10.
(43) Szleifer, I. *Biophys. J.* **1997**, *72*, 595−612.
(44) Guffond, M. C.; Williams, D. R. M.; Sevick, E. M. *Langmuir* **1997**, *13*, 5691−5696.
(45) Jimenez, J.; Rajagopolan, R. *Langmuir* **1998**, *14*, 2598−2601.
(46) Dolan, A.; Edwards, F. *Proc. R. Soc. London* **1974**, *337*, 509−516.

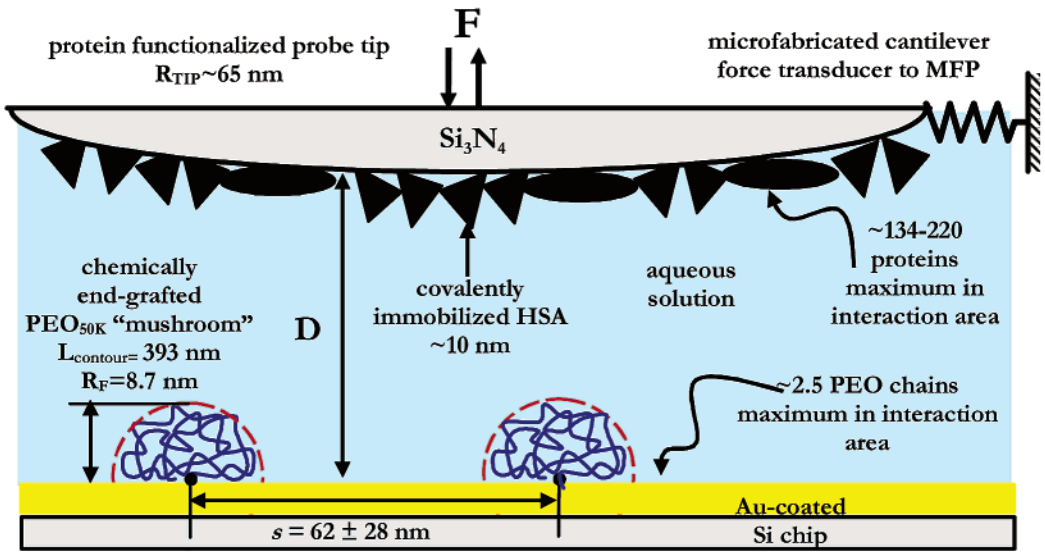

Figure 2. HRFS experimental setup.

To summarize, the possible repulsive forces present include steric forces, enthalpic penalties for disruption of hydrogen bonds with water, electrostatic double layer forces, and hydrodynamic lubrication forces.

PEO: Attractive Interactions with Proteins. Attractive protein−polymer interactions may include hydrogen bonding, electrostatic, and van der Waals (VDW) forces (e.g., including the so-called "hydrophobic" interactions). The hydrophobic character of PEO is supported by its known solubility in both aqueous and organic solvents,[23] adsorption to hydrophobic surfaces and the air−water interface,[48−52] and its use as a surfactant in a number of applications.[53−56] The noncovalent complexation between PEO and the blood plasma protein human serum albumin in dilute aqueous solution has been studied via quasi-elastic light scattering, static light scattering, electrophoretic light scattering, dialysis, and fluorescence spectroscopy under a variety of conditions and for a series of different PEO molecular weights.[16] Complexation is observed to occur at low pH, presumably due to hydrophobic interactions supported by hydrogen bonding between the ether groups of the PEO with the carboxyl and phenolic −OH groups in the protein. Complexation also occurs at high pH since most of the basic groups in the HSA are deprotonated and can also form hydrogen bonds with the ether groups of the PEO.

Direct Measurement of Protein−PEO Interactions. This report focuses on investigating the molecular origins of PEO hemocompatibility using the powerful technique of high-resolution force spectroscopy (HRFS). Human serum albumin (HSA), the most abundant blood plasma protein and typically the first to adsorb to the surfaces of implanted biomaterials,[57] was covalently grafted to a silicon nitride (Si_3N_4) probe tip of end radius $R_{tip} \sim 65$ nm, at the end of a soft, microfabricated cantilever force transducer. Relatively long mono(thiol)-terminated PEO chains ($M_n \approx 50$K, contour length $L_{contour} \approx 393$ nm, Flory radius $R_F \sim 9$ nm in aqueous solution) were covalently end-grafted to gold surfaces at low density, that is, in the mushroom regime ($s > 2R_F$ where s is the distance between end-grafting sites and is ~62 nm), yielding an areal chain packing of $\Gamma \sim 0.00026$ chains/nm^2. In the mushroom regime, the theoretical average height of the polymer chain is $\sim R_F$. The net nanoscale force versus separation distance between this HSA-modified probe tip and the PEO-modified surface was measured directly on approach and retract in aqueous buffer solution using HRFS as shown in Figure 2. Using the methodology described previously,[58] the HSA-modified probe tip used in this study was calculated to have a small maximum surface interaction area at a tip−surface separation distance D = 0 of 6100 nm^2 = 0.0061 μm^2, which corresponds to ~220 HSA proteins assuming a triangular shape,[59−61] or ~134 HSA proteins assuming an ellipsoidal shape lying flat,[62−64] for a close-packed monolayer, as compared to the crossed cylinder geometry of a similar technique, the surface force apparatus (SFA), which has a surface interaction area of ~100 μm^2, corresponding to $>2.2 \times 10^6$ HSA molecules.[17,65] For the substrate, a maximum surface interaction area at D = 0 of 9500 nm^2 = 0.0095 μm^2 was calculated, corresponding to ~2.5 PEO chains under the probe tip.[58] The soft microfabricated cantilever used as the force transducer in our nanomechanical apparatus, the Molecular Force Probe[66] (MFP),

(47) Fredrickson, G. H.; Pincus, P. *Langmuir* **1991**, *7*, 786.
(48) Wu, S. *Polymer Interfaces and Stability*; Marcel Dekker: New York, 1982.
(49) Israelachvili, J.; Adams, G. E. *J. Chem. Soc., Faraday Trans. 1* **1978**, *74*, 975−1001.
(50) Kretschmann, E.; Rather, H. *Z. Naturforsch.* **1968**, *Teil A 241*, 2135−2136.
(51) Kretschmann, E. *Z. Phys.* **1971**, *241*, 313−324.
(52) Lavrik, N. A.; Leckband, D. *Langmuir* **2000**, *16*, 1842−1851.
(53) Mahn, W. K. *Colloids Surf., A* **1997**, *128*, 145−154.
(54) Ahrens, H.; Baekmark, T. R.; Merkel, R.; Schmitt, J.; Graf, K.; Raiteri, R.; Helm, C. A. *ChemPhysChem* **2000**, *1*, 101.
(55) Cao, B.; Kim, M. W. *Faraday Discuss.* **1994**, *98*, 245.
(56) Kim, M. *Colloids Surf., A* **1997**, *128*, 145.
(57) Vroman, L.; Adams, A. L. In *Why Plasma Proteins Interact at Interfaces*; Brash, J. L., Horbett, T. A., Eds.; Washington, DC, 1987.
(58) Rixman, M. A.; Dean, D.; Macias, C. E.; Ortiz, C. *Langmuir* **2003**, *19*, 6202−6218.
(59) Curry, S.; Mandelkow, H.; Brick, P.; Franks, N. In *Brookhaven Protein Databank*: http://www.rcsb.org/pdb.
(60) Curry, S.; Mandelkow, H.; Brick, P.; Franks, N. *Nat. Struct. Biol.* **1998**, *5*, 827.
(61) Carter, D. C.; Ho, J. X. *Adv. Protein Chem.* **1994**, *45*, 153−204.
(62) Haynes, C. A.; Norde, W. *Colloids Surf., B* **1994**, *2*, 517.
(63) Peters, T. *Adv. Protein Chem.* **1985**, *37*, 161.
(64) Soderquist, M. E.; Walton, A. G. *J. Colloid Interface Sci.* **1980**, *75*, 386.
(65) Efremova, N. V.; Sheth, S.; Leckband, D. *Langmuir* **2001**, *17*, 7628−7636.
(66) Asylum Research, I. S. B., Santa Barbara, CA. URL: http://www.asylumresearch.com.

has a low limit of force detection of ±5 pN in fluids. Both of these features enable many interesting observations to be made, including the measurement of HSA adhesive binding to individual PEO macromolecules. The approach data were analyzed through a comparison with molecular level theoretical models for the individual constituent components of the total net force, including van der Waals, electrostatic double layer, and configurational entropy, and the retract data were analyzed via fits to single molecule elasticity theories. Similar to many cantilever-based instruments such as the atomic force microscope (AFM), the MFP does not have an absolute measurement of the probe tip−surface separation distance and the probe tips employed can have highly variable geometry. Both of these factors will be discussed in detail in the experimental section of this paper. Our long-term objective is to develop rigorous experimental and theoretical approaches needed to understand, and possibly assess, macromolecular biocompatibility at the nanoscale and to use this information as a guideline for the design of improved synthetic macromolecular systems for biomedical applications. This study also has a broader significance in the context of presenting new methodologies for macromolecular nanoscale adhesion and in other areas such as colloid stabilization, marine biofouling, and selective deposition of polyelectrolytes.

Experimental Methods

Control Experiments: HSA Probe Tip on a Gold Substrate. In our recent paper,[58] we reported the nanoscale intermolecular forces between a 65 nm radius probe tip covalently grafted with HSA and a polycrystalline gold substrate in phosphate-buffered saline (PBS) solution (ionic strength IS = 0.01 M, pH = 7.4), the results of which are also employed in this report. Preparation and characterization of the HSA probe tip and gold substrates, as well as detailed analysis of the experimental results, were reported previously.[58] The same exact cantilever (Thermomicroscopes, Inc. V-shaped Si_3N_4 cantilever with a spring constant $k_c \sim 0.01$ N/m) and HSA-modified probe tip ($R_{tip} \sim 65$ nm as measured by scanning electron microscopy (SEM)) used in the previously cited reference[58] were used for all experiments presented in this paper on the same day of experimentation. To summarize the relevant results for the readers' convenience, it was found that the HSA-modified probe tip exhibited a purely repulsive, nonlinear force on approach to the Au substrate which, based on Derjaguin−Landau−Verwey−Overbeek (DLVO) theoretical models,[67,68] is believed to be predominantly due to electrostatic double layer forces. It was determined that the HSA probe tip possessed a net negative charge of -0.0064 C/m^2 and that the Au substrate also possessed a net negative charge of -0.014 C/m^2 (possibly due to adsorbed anions). On retraction, the HSA and Au exhibited surface adhesion and the average forces and distances of adhesion were $\langle F_{adh} \rangle = 1.35 \pm 0.19$ nN, $\langle F_{adh} \rangle / R_{tip} = 21 \pm 2.9$ nN (where R_{tip} is the end radius of curvature of the probe tip), and $\langle D_{adh} \rangle = 22.5 \pm 6.3$ nm (n = 46 datapoints).

HRFS Experiments. All HRFS experiments were conducted using a new cantilever-based instrument, the Molecular Force Probe (Asylum Research, Santa Barbara, CA) to measure force, F (nN), versus tip−sample separation distance, D (nm) (henceforth referred to and labeled on graphs as "Distance"), on "approach" (i.e., probe tip advancing toward surface) and "retract" (i.e., probe tip moving away from surface). A full description of this instrument, its limits of force and displacement detection in fluids, procedures for spring constant calibration and conversion of raw data, details of measurement errors, and description of typical force versus distance curves including the mechanical instabilities of the cantilever are given in our previous works.[58,69,70] The accuracy of the D = 0 position is described in the Appendix, and based on the discussion therein, it is expected that steric deformations of the protein have negligible contribution to the interaction force profile on approach. All experiments were conducted in PBS (pH = 7.4, IS = 0.01 M) under the same experimental conditions described previously.[58] The PBS solutions were made using sodium phosphate buffer tablets (Sigma lot no. 59H03371), which contain 8 g/L NaCl, 0.2 g/L $K^+H_2PO_4^-$, 1.15 g/L $2Na^+ \cdot HPO_4^{2-}$, and 0.2 g/L KCl, and were diluted to obtain an ionic strength of 0.01 M. Importantly, the HRFS experimental data were averaged over many HRFS experiments and presented always with standard deviations and normalized by the probe tip radius, giving a representative effective energy of interaction.

End-Grafting and Characterization of Poly(ethylene oxide) to Gold Substrates. Linear PEO_{50K}-SH, $M_n = 48\,320$ g/mol, $M_w = 51\,700$ g/mol, PDI = 1.07 (as determined by gel permeation chromatography (GPC) in tetrahydrofuran using monodisperse poly(ethylene glycol) standards), was custom synthesized by Polymersource, Inc. (lot no. P2415-EOSH). R_F in aqueous solution was calculated to be ∼8.7 nm from Flory statistical mechanics using the equation $R_F = \alpha l_{C-O}(C_\infty N/3)^{1/2}$, where $\alpha^5 - \alpha^3 = 2C_M[0.5 - \chi](M_n)^{1/2}$,[71] l_{C-O} is the carbon−oxygen bond length (=0.143 nm), $C_\infty \sim 4$ is the characteristic ratio,[28] $C_M = 0.175$ is a constant,[28] $\chi = 0.42$ at ∼25 °C,[28] $\alpha = 1.59$ is the Flory expansion parameter and measures the degree of swelling in a solvent, and N = 1098 is the number-average number of repeat units in the polymer chain. The contour length, $L_{contour}$, was calculated to be 393 nm from the polymer number-average molecular weight using the all-trans segment length of 0.358 nm, assuming a C−O bond length of 0.143 nm, a C−C bond length of 0.158 nm, and bond angles of 109.5°. PEO_{50K}-SH was chemisorbed to 1 cm^2 polycrystalline gold-coated Si wafers by immersing the wafers for 45 min in 2 mL of 10 μM solutions of PEO in deionized (DI) H_2O. Physisorbed chains were then removed from each substrate by repeated, vigorous rinsing with a steady stream of DI H_2O, and the samples were immediately stored in glass vials containing filtered DI H_2O. The polymer concentration of the stock solution was well below the critical overlap concentration, c* = 0.6 mM, or 0.0291 g/mL, calculated from the equation $c^* = 3M_n/(4N_A\pi R_F^3)$ where N_A is Avogadro's number. All of these properties of PEO_{50K} are summarized in Table 1.

Contact mode fluid AFM images taken using a Digital Instruments Nanoscope IIIA Multimode of a bare Au substrate (Figure 3A)[72] compared to PEO-grafted surfaces (Figure 3B) have allowed for the identification of isolated, individual PEO chains similar to refs 73 and 74. The gold root-mean-square surface roughness, island size, and island peak-to-valley height were found to be ∼1.2 nm, ∼30 nm, and ∼3.5 nm, respectively. Generally, the hemispherical gold grain caps seen clearly in Figure 3A are much larger and more rigid (i.e., incompressible with the soft cantilevers used here for imaging) than the much smaller, softer, globular features (which easily distort and become "blurry" with increasing imaging force) identified in Figure 3B as the PEO mushrooms. The distance between two polymer chains was calculated using the "Section Analysis" command in the image analysis software package of the AFM. A line was drawn between the centers of two polymer chains across the image, and the two-dimensional topography was mapped along this line. Cursors were then placed on the two points of interest, and the distance between them was recorded. The piezoelectric scanner was calibrated in all three coordinate axes using a 10 × 10 μm^2

(67) Derjaguin, B. V.; Landau, L. D. *Acta Physiochim. URSS* **1941**, *14*, 633.

(68) Verwey, E.; Overbeek, W. J. T. *Theory of Stability of Lyophobic Colloids*; Elsevier: Amsterdam, The Netherlands, 1948.

(69) Jiang, X.-P.; Ortiz, C.; Hammond, P. *Langmuir* **2002**, *18*, 1131−1143.

(70) Seog, J.; Dean, D.; Grodzinsky, A.; Plaas, A.; Wong-Palms, S.; Ortiz, C. *Macromolecules* **2002**, *35*, 5601−5615.

(71) Flory, P. J. *Statistical Mechanics of Chain Molecules*; Hanser: Munich, 1988.

(72) Figure 3A was originally reported by us in: Seog, et al. *Macromolecules* **2002**, *35* (14), 5601−5615. In this reference, there was an error describing the figure: this image was taken in PBS rather than in air.

(73) Koutsos, V.; van der Vegte, E. W.; Grim, P. C. M.; Hadziiouannou, G. *Macromolecules* **1998**, *31*, 116.

(74) Koutsos, V.; van der Vegte, E. W.; Hadziiouannou, G. *Langmuir* **1999**, *32*, 1233.

Table 1

symbol (units)	property	value	method
FW (g/mol)	formula weight	44	addition of constituent atomic weights
$l_{monomer}$ (ttg) (nm)	mean monomer length (trans-trans-gauche)	0.278	crystallography[34]
$l_{monomer}$ (ttt) (nm)	monomer length (trans-trans-trans)	0.358	planar zigzag backbone estimated with bond lengths[34]: $l_{C-C} = 0.154$ nm, $l_{C-O} = 0.143$ nm
C_∞	characteristic ratio	4	see ref 40
χ	Flory−Huggins interaction parameter in water	0.42	see ref 40
C_M	expansion constant	0.175	see ref 40
M_n (g/mol)	number average molecular weight	48500	GPC
M_w (g/mol)	weight average molecular weight	51700	GPC
PDI	polydispersity index = M_w/M_n	1.07	GPC
N	number of monomers	1102	$N = M_n/FW$
$L_{contour}$ (ttt) (nm)	contour length (ttt)	393	$L_{contour} = N l_{monomer}$(ttt)
α	Flory expansion parameter	1.60	$\alpha^5 - \alpha^3 = 2C_M(0.5 - \chi)MW^{1/2}$
R_F (nm)	Flory radius in water	8.7	$R_F = \alpha\, l_{C-O}(C_\infty N/3)^{1/2}$
c* (M)	critical overlap concentration in solution	0.6	$c^* = 3M_n/4N_A\pi R_F^3$

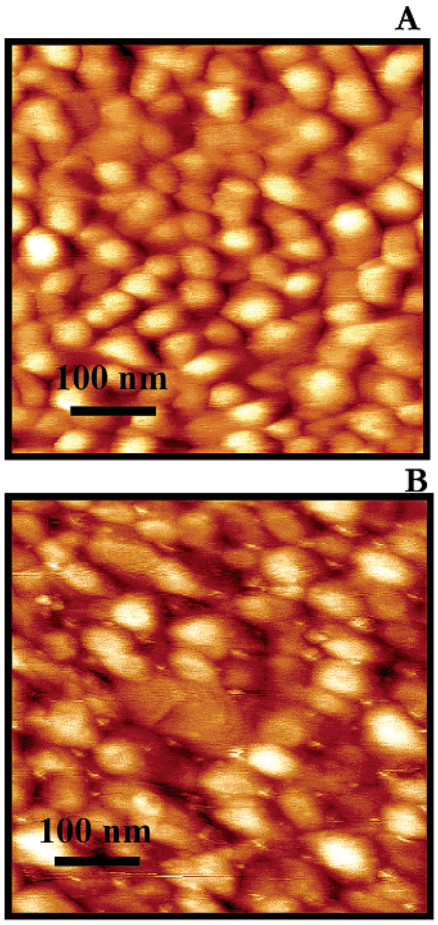

Figure 3. Contact mode AFM images in PBS solution of (A) a bare polygranular gold substrate[72] and (B) a polygranular gold substrate modified by covalent attachment of PEO_{50K}.

(*xy*) calibration grid in addition to 5 nm diameter Au beads on a cleaved mica surface (*y*). The distance between neighboring polymer chains, $s = 62 \pm 26.8$ nm, is much greater than $2R_F$ and corresponds to the presence of ~2.5 polymer chains within the maximum tip−surface interaction area at D = 0.[58] Under these conditions, the polymers are in the mushroom state.[75] The dimensions of the individual polymer chain mushrooms were found to be consistent with the known R_F for PEO_{50K}: a length perpendicular to the scan direction of 7.9 ± 2.2 nm, a length parallel to the scan direction of 18.5 ± 3.8 nm, and a height of $h < 5$ nm. Since the polymer chains are unavoidably compressed and dragged by the probe tip in contact mode even under low force imaging, there was a consistent elongation in the scan direction, as well as a reduced height (i.e., $h < R_F$). Contact angle measurements were performed using deionized water and a VCA 2000 Video Contact Angle System apparatus. The advancing contact angle was found to be 60 ± 1°, and the receding contact angle was found to be 22 ± 1°. Table 2 summarizes the maximum distance of interaction on approach (D_{max}), the maximum (at D = 0) probe tip and substrate interaction areas (A_{tip}, $A_{substrate}$), the number of proteins and PEO chains contained within each of these areas, respectively (which were detailed in the Introduction), the maximum compressive force per protein within the maximum probe tip−surface interaction area (F_{max} < 22 pN, much less than the expected force needed for mechanical denaturation of HSA),[76] and the Hertzian elastic contact area ($A_{contact}$ = 5.5 nm^2), which were calculated as described previously.[58]

Table 2

D_{max} (nm)	30
R_{tip} (nm)	65
s (nm)	62
Γ (chains/nm^2)	0.00026
A_{tip} (HSA) (nm^2) at D = 0	6100
$A_{substrate}$ (nm^2) at D = 0	9500
$A_{triangle}$ (HSA) (nm^2)	28
$A_{ellipse}$ (HSA) (nm^2)	45
no. of proteins in A_{tip} (assuming a triangularly shaped protein) at D = 0	220
no. of proteins in A_{tip} (assuming an ellipsoidally shaped protein) at D = 0	134
no. of PEO chains in $A_{substrate}$ at D = 0	2.5
F_{max} (nN)	3
F_{max}/protein (assuming a triangularly shaped protein) (pN) at D = 0	14
F_{max}/protein (assuming an ellipsoidally shaped protein) (pN) at D = 0	22
$A_{contact}$ (nm^2)	5.5

Results

I. Interaction of HSA Probe Tip versus PEO-Modified Au Surface on Approach. Figure 4 displays the average F/R_{tip} (mN/m) versus Distance, D (nm), approach curves for an HSA probe tip versus PEO end-grafted on Au (denoted PEO−Au and graphically represented by black diamond symbols) compared to Au (represented by red squares) and CH_3-terminated and COO^--terminated alkanethiol self-assembled monolayer (SAM) surfaces (represented by blue triangles and green circles, respectively) in PBS solution, as well as the corresponding standard deviations for each dataset. For the PEO−Au sample, nonlinear, purely repulsive forces were observed to begin at D < 30 nm, reaching a maximum magnitude at D = 0 of $F/R_{tip} \sim 6.6$ mN/m before reaching the constant compliance regime with no attractive jump-

(75) Flory, P. J. *Principles of Polymer Chemistry*; Cornell University Press: Ithaca, NY, 1953.
(76) Erickson, H. P. *Science* **1997**, *276*, 1090−1092.

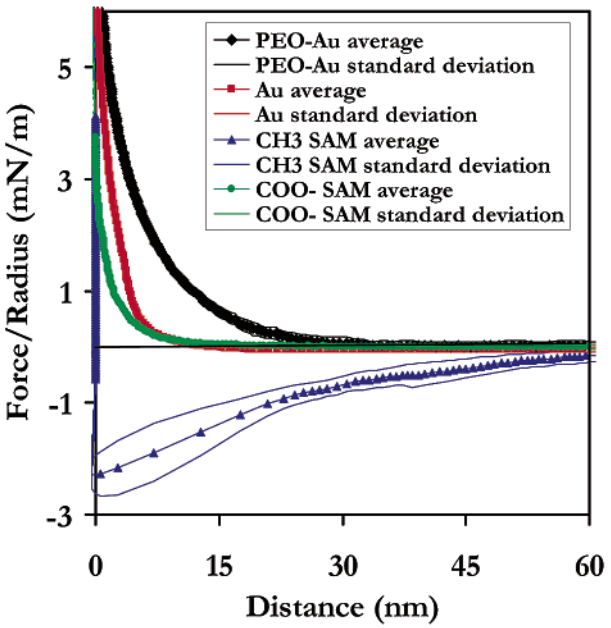

Figure 4. Average Force/Radius (mN/m) versus Distance (nm), approach curves for an HSA probe tip on PEO_{50K}−Au (black diamonds), gold (red squares), CH_3-terminated SAM (blue triangles), and COO^--terminated SAM (green circles) surfaces in PBS solution, as well as standard deviations.

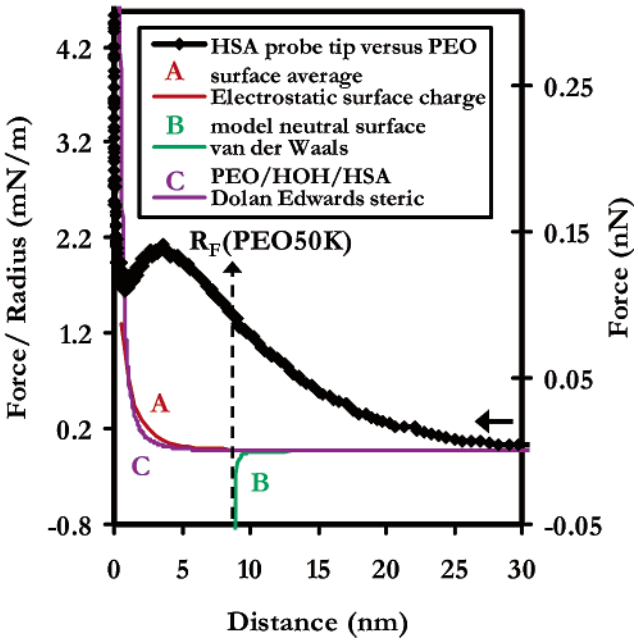

Figure 5. Averaged Force (nN) and Force/Radius (mN/m) versus Distance (nm), of an HSA probe tip on approach to a PEO_{50K}−Au substrate in PBS solution, for which 94% of the averaged approach curve of HSA probe tip vs bare Au surface has been subtracted so that the curve represents only HSA−PEO interactions. The experimental data are compared to: (A) a constant surface charge model[70] between an impermeable, hemispherical HSA-grafted probe tip of radius 65 nm and constant surface charge $\sigma_{tip} = -0.0064$ C/m^2 and a neutral ($\sigma_{plane} = 0$), flat PEO surface (red line); (B) the van der Waals attractive force between a PEO mushroom and an HSA-grafted probe tip in an aqueous medium (green line); and (C) the Dolan−Edwards model for steric repulsion at short distances,[46] between an incompressible probe tip of radius 65 nm and a PEO mushroom of $R_F = 8.7$ nm, $L_{contour} = 393$ nm, and a mean area per PEO molecule of $s^2 = 3844$ nm^2 (purple line).

to-contact. As a first-order approximation, additivity is assumed so that this measured net interaction is a linear superposition of the HSA probe tip interaction with the underlying Au substrate plus that of the PEO chain(s):

$$F(D)_{HSA/PEO-Au} = F(D)_{HSA/Au} + F(D)_{HSA/PEO} \quad (1)$$

To approximate the HSA versus PEO interaction, 94% of the magnitude of the HSA versus Au curve (Figure 4, red square symbols) (i.e., the average percentage of the PEO-grafted substrate that is not covered by PEO) was subtracted from the HSA versus PEO−Au (Figure 4, black diamond symbols), yielding the curve shown in Figure 5 (black triangular symbols, henceforth referred to as HSA versus PEO dataset). The assumption of additivity in eq 1 is based on the approximation that the presence of the small amount of end-grafted PEO does not significantly alter the surface charge per unit area on the bare Au regions of the substrate (which is presumably due to anion adsorption) and gives rise to the respulsive electrostatic double layer force. Given the extremely low coverage of PEO on the surface (6% of the total surface area), we feel that this is a reasonable approximation. The data greater than the range of the gold interaction, that is, $D > 13$ nm, have not undergone any subtraction manipulation and are of great interest; these data are discussed in detail below.

In Figure 5, we see that the HSA versus PEO force curve also shows a nonlinear, purely repulsive force beginning at $D < 30$ nm, but also exhibits a local maximum (force barrier) at $D = 3.6$ nm corresponding to 2.1 mN/m and 0.14 nN, after which the force decreases with decreasing separation distance to 1.5 mN/m and 0.09 nN at $D = 0$ (i.e., the constant compliance regime). As mentioned in the Introduction, the net HSA versus PEO interaction on approach may have multiple components including electrostatic double layer, steric, van der Waals, hydration, and hydrodynamic lubrication forces. Figure 5 compares these experimental data for the HSA probe tip versus PEO chain(s) to a variety of theoretical curves showing the magnitudes, ranges, and forms of these possible force constituents. Each one of these theoretical curves was calculated based on known parameters and is described in detail below.

Electrostatic Double Layer Forces. The electrostatic double layer component of the force was modeled using a constant surface charge approximation based on the numerical solution to the nonlinear Poisson−Boltzmann (PB) equation including divalent ions[70,77,78] in which the PEO substrate is assumed to have neutral charge (σ_{plane}(PEO) = 0 C/m^2) and the HSA probe tip is modeled as an impermeable hemisphere of radius R_{hemis}, also with constant charge per unit area (σ_{tip}(HSA) = −0.0064 C/m^2, determined from previous experiments[58]). The force was obtained from the electrical potential, Φ, using the free energy method[77,79,80] and surface element integration (SEI).[81] In the theoretical data fits, the electrical interaction Debye length, κ^{-1}, was set to its known value for IS = 0.01 M ($\kappa^{-1} = 2.96$ nm), R_{hemis} was fixed to the known value of R_{tip} measured by SEM (=65 nm), and there were no fitting parameters. Figure 5A (red line) shows that a relatively small, purely repulsive force is predicted even though σ_{plane} of the substrate has been set to zero since the

(77) Dean, D.; Seog, J.; Ortiz, C.; Grodzinsky, A. *Langmuir* **2003**, *19*, 5526−5539.
(78) Ninham, M.; Parsegian, A. *J. Theor. Biol.* **1971**, *31*, 405−428.
(79) Sharp, K. A.; Honig, B. *J. Phys. Chem.* **1990**, *94*, 7684−7692.
(80) Jin, M.; Grodzinsky, A. J. *Macromolecules* **2001**, *34*, 8330−8339.
(81) Bhattacharjee, S.; Elimelech, M. *J. Colloid Interface Sci.* **1997**, *193*, 273−285.

tip and substrates are large compared to κ^{-1} and they are impermeable to ions.[82]

van der Waals Interaction. The van der Waals interaction between the hydrated PEO mushroom layer on the surface and the HSA layer on the probe tip was calculated using the inverse square power law (eq 2) derived using the "Derjaguin approximation" (which is valid for $D \ll R$):[83]

$$F_{VDW}(D) = -\frac{AR}{6D^2} \quad (2)$$

where F_{VDW} is the van der Waals force between a sphere of radius R (assumed to be equal to the probe tip radius, R_{tip}) and a planar surface separated by a distance D, and *A* is the nonretarded Hamaker constant, which was fixed. $F_{VDW}(D)$ is plotted in Figure 5B (green line). An approximate expression for the nonretarded Hamaker constant, A_{132}, between two macroscopic media 1 (hydrated PEO mushroom layer) and 2 (HSA layer) interacting across medium 3 (HOH) is given by the Lifshitz continuum theory[84] and, for bare surfaces, is known to correlate with experimentally measured van der Waals adhesion energies at separation distances of 0.5 nm:[85]

$$A_{132} \approx \frac{3k_BT}{4}\frac{(\epsilon_1-\epsilon_3)}{(\epsilon_1+\epsilon_3)}\frac{(\epsilon_1-\epsilon_2)}{(\epsilon_1+\epsilon_2)} + \frac{3h\nu_e}{8\sqrt{2}} \times \frac{(\eta_1^2-\eta_3^2)(\eta_2^2-\eta_3^2)}{(\eta_1^2+\eta_3^2)^{1/2}(\eta_2^2+\eta_3^2)^{1/2}[(\eta_1^2+\eta_3^2)^{1/2}+(\eta_2^2+\eta_3^2)^{1/2}]} \quad (3)$$

where ϵ is the dielectric constant, η is the refractive index, h is Planck's constant ($=6.626 \times 10^{-34}$ J·s), and ν_e is the electronic absorption frequency in the UV ($=3 \times 10^{15}\ s^{-1}$).[84] The dielectric constant and refractive index of the uncompressed, hydrated polymer mushroom layer were calculated using:[86]

$$\eta_1 = \phi_{PEO}\eta_{PEO} + \phi_{HOH}\eta_{HOH}$$
$$\epsilon_1 = \phi_{PEO}\epsilon_{PEO} + \phi_{HOH}\epsilon_{HOH} \quad (4)$$
$$1 = \phi_{PEO} + \phi_{HOH}$$

where $\epsilon_{PEO} = 3.5$, $\epsilon_{HOH} = 80$, $\eta_{PEO} = 1.45$, and $\eta_{HOH} = 1.33$. The average volume fractions of PEO and HOH were calculated from the PEO chain grafting density, $\Gamma = 0.00026$ chains/nm^2, and the density of PEO in the solid state, $\rho_{PEO} = 1.2$ g/cm^3, yielding $\phi_{PEO} = 0.0020$. η_1 was calculated to be 1.33 and ϵ_1 to be 79.85 from eq 4, both dominated by water due to the low chain grafting density. For the HSA layer on the probe tip, η_2 was taken to be 1.47[87] and ϵ_2 to be 2.5.[88] Using these values, A_{132} was calculated to be 1.26×10^{-22} J and the outer van der Waals plane was assumed to be equal to R_F. As shown in Figure 5B (green line), a relatively weak attractive force is predicted which would lead to a jump-to-contact at the top of the polymer mushroom layer. PEO is predicted to have the lowest van der Waals interaction when compared to other common water-soluble synthetic polymers.[89] This prediction is qualitative at best due to the assumptions of a constant dielectric constant throughout the PEO and HSA layers, a constant PEO segment density profile which exhibits a sharp cutoff at the equilibrium mushroom height, and underlying substrate surface roughness, all of which result in an overestimation of the van der Waals force.[17] Such an attractive jump-to-contact has been observed previously for high grafting density poly(L-glutamic acid) brushes measured via the SFA,[90] but was most likely too small to be observed here experimentally. A finite attraction is theoretically predicted at contact (rather than the infinite attraction for uniform dielectric layers described by the Lifshitz theory), because the dielectric properties of the diffuse outer layers of the polymer layer at the surface decay to those of water at the outer edge.[91]

Configurational Entropy Force. Figure 5C (purple line) shows the Dolan−Edwards theory for the repulsive interaction between a rigid, planar surface and a dilute layer of end-grafted, noninteracting mushrooms on an opposing planar surface.[46] This theory is based on the configurational entropy loss of ideal random flight (flexible) polymer chains, and the force in a good solvent can be solved analytically and converted to the appropriate geometry for these experiments via the Derjaguin approximation (valid for $D \ll R_{tip}$):

$$F_{mushroom} = 2\pi R_{tip}\Gamma k_BT\left[\frac{\pi^2\langle R_F\rangle^2}{6D^2} + \ln D\left(\frac{3}{8\pi\langle R_F\rangle^2}\right)^{1/2}\right], \quad D < 1.73\langle R_F\rangle \quad (5)$$

Excluded volume interactions are taken into account indirectly through $\langle R_F\rangle$.

Hydration or Structural Forces. A very short range (<4 nm), monotonic, exponentially repulsive force has been observed experimentally between a variety of different smooth, hydrophilic, charged surfaces in electrolyte solutions of intermediate and high ionic strength.[84] The origin of this force has been quite controversial and is generally attributed to the displacement of hydrated, adsorbed surface counterions and is due to the energy needed to dehydrate the bound counterions, which retain some of their water of hydration on binding. Presumably, this force is highly sensitive to, and will decrease with, increasing surface roughness. As mentioned in the Introduction, HSA is known to have a 0.55 nm thick monolayer of closely associated water molecules on its surface, with most (98%) oriented with their H atoms pointed toward the protein surface. The next layer of water is about 30% oriented, creating a "fuzzy" hydrated interphase in aqueous solution.[92]

II. Interaction of HSA Probe Tip versus PEO-Modified Au Surface on Retract. *General Description of Force Curves.* Figure 6 plots typical individual F (nN) and F/R_{tip} (mN/m) versus D (nm) approach and retract curves for an HSA probe tip versus a PEO−Au surface in PBS solution. Retraction of the probe tip away from the substrate almost always yielded a nonhysteretic

(82) Parsegian, V. A.; D., G. *Biophys. J.* **1972**, *12*, 1192−1204.
(83) Derjaguin, B. V. *Kolloid-Z.* **1934**, *69*, 155−164.
(84) Israelachvili, J. N.; Adams, G. E. In *Intermolecular and Surface Forces*, 2nd ed.; Academic Press: San Diego, 1992.
(85) Langbein, D. *Theory of van der Waals Attraction*; Springer Tracts in Modern Physics, Vol. 72; Springer-Verlag: Berlin, 1974.
(86) Jeon, S. I.; Andrade, J. D. *J. Colloid Interface Sci.* **1991**, *142*, 159−166.
(87) Brynda, E.; Houska, M.; Wikerstal, A.; Pientka, Z.; Dyr, J. E.; Bradenburg, A. *Langmuir* **2000**, *16*, 4352−4357.
(88) Grymonpré, K.; Staggemeir, B.; Dubin, P. L.; Mattison, K. W. *Biomacromolecules* **2001**, *2*, 422.
(89) Jeon, S. I.; Lee, J. H.; Andrade, J. D.; DeGennes, P. G. *J. Colloid Interface Sci.* **1991**, *142*, 149−158.
(90) Abe, T.; Higashi, N.; Niwa, M.; Kurihara, K. *Langmuir* **1999**, *15*, 7725−7731.
(91) Bevin, M. A.; Prieve, D. C. *Langmuir* **2000**, *16*, 9274−9281.
(92) Peters, T. *All About Albumin*: *Biochemistry, Genetics, and Medical Applications*; Academic Press: San Diego, 1992.

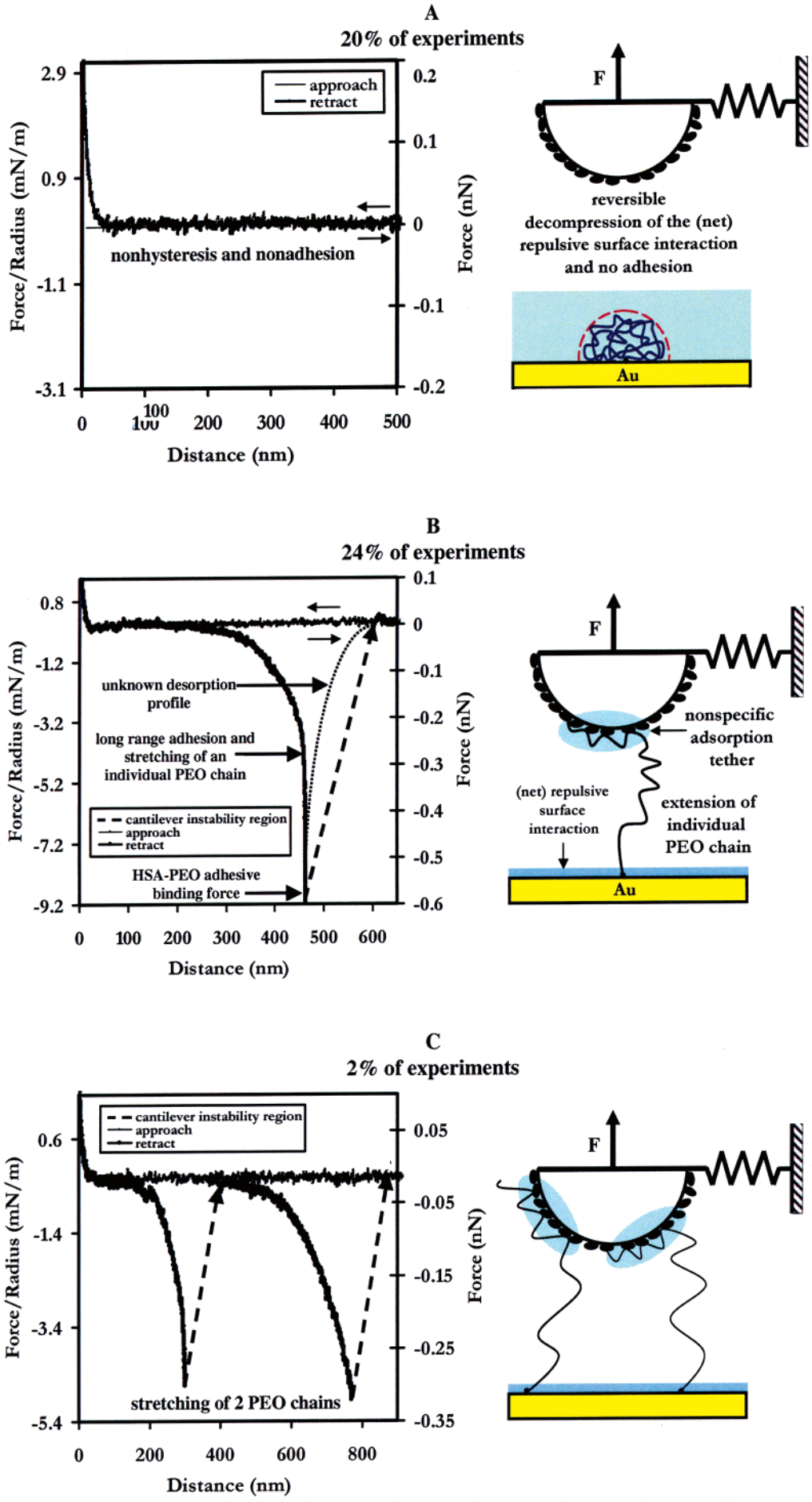
A
20% of experiments
approach
retract
nonhysteresis and nonadhesion
Force/Radius (mN/m)
Force (nN)
Distance (nm)
F
reversible
decompression of the (net)
repulsive surface interaction
and no adhesion
Au
B
24% of experiments
unknown desorption
profile
long range adhesion and
stretching of an
individual PEO chain
cantilever instability region
approach
retract
HSA-PEO adhesive
binding force
nonspecific
adsorption
tether
(net) repulsive
surface
interaction
extension of
individual
PEO chain
Au
C
2% of experiments
cantilever instability region
approach
retract
stretching of 2 PEO chains

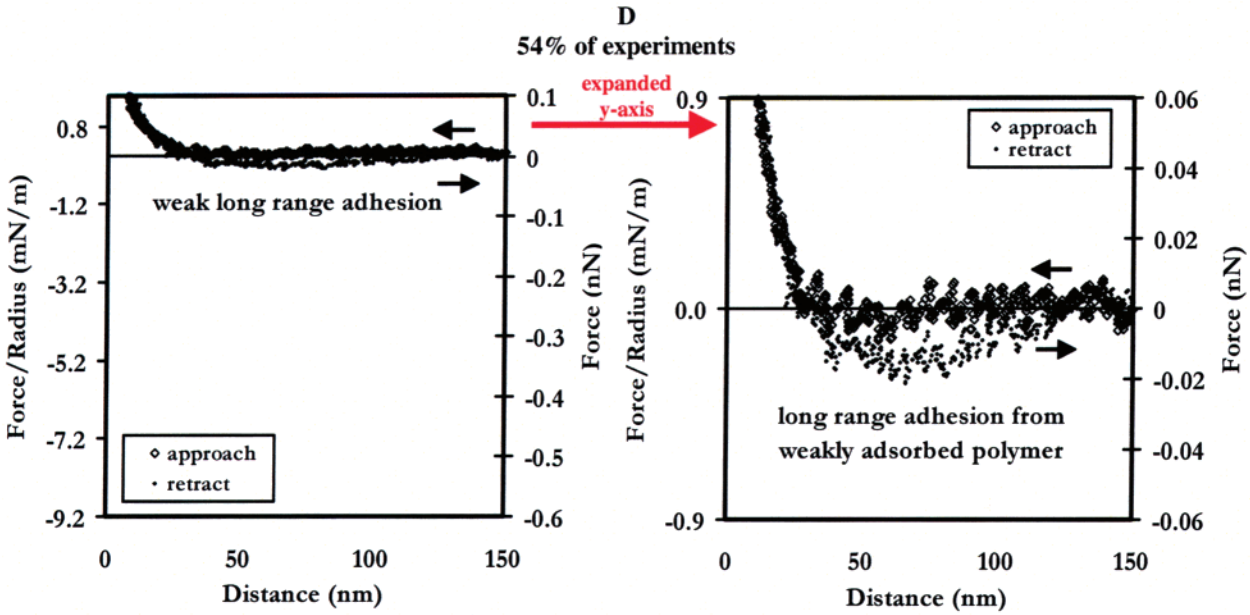

Figure 6. Typical individual Force (nN) (linear scale) versus Distance (nm) retraction curves of an HSA probe tip from a PEO_{50K}–Au substrate in PBS solution and their relative frequencies of occurrence: (A) nonadhesion; (B) extension of an individual, strongly adsorbed PEO chain; (C) extension of two strongly adsorbed PEO chains; and (D) extension of an individual, weakly adsorbed PEO chain.

interaction profile for D < 30 nm, indicating minimal interaction of the PEO chain with the underlying Au substrate and near-complete elimination of short-range surface adhesion (1% of the data exhibited surface adhesion). Curves similar to Figure 6A were observed in 20% of the force spectroscopy experiments, while those similar to Figure 6B were observed in 24% of the force spectroscopy experiments, those in Figure 6C were observed in 2%, and those in Figure 6D were observed in 54% of the force spectroscopy experiments (a total of n = 318 force curves were taken). Figure 6B shows an individual, long-range, attractive peak in which the magnitude of the force increases nonlinearly with distance. This peak is attributed to the stretching of an individual PEO chain that had become strongly physically adsorbed to the HSA probe tip on approach and bridges the substrate and tip. At high enough extensions, the elastic restoring force of the chain becomes equal to and just exceeds the physisorption force tethering the chain segments to the tip and the tethered chain segments detach from the probe tip. Upon detachment, the cantilever exhibits a mechanical instability and is returned back to its undeflected position corresponding to zero force. The mechanical instability of the cantilever hides an unknown desorption interaction profile between the adsorbed PEO chain segments and the HSA proteins on the probe tip. The detachment or desorption force represents the adhesive binding interaction between an individual PEO chain and the HSA probe tip. As is shown in Figure 6C, a small number of the experiments performed exhibited two attractive peaks, most likely corresponding to two strongly adsorbed PEO chains. As shown in Figure 6D, 54% of the total HRFS exhibited a weak long-range adhesion with a gradual detachment back to the zero force baseline rather than a distinct desorption event and cantilever instability. It is suspected that these curves represent an individual polymer bridging chain that is only weakly adsorbed to the probe tip and undergoes a small amount of extension as the tip retracts.

Comparison to Single Molecule Elasticity Theories. Figure 7A overlays multiple retraction curves from numerous force spectroscopy experiments, and Figure 7B normalizes the *x*-axis of these multiple experiments by the contour lengths of the bridging chains in order to create a master curve which represents the molecular elasticity of the macromolecules.[93] This master curve was compared to the extensible freely jointed chain model[94] (Figure 7B, solid red line), which is known to describe well the extension behavior of a single molecule of PEO stretched by a bare Si_3N_4 probe tip in a nonpolar solvent (e.g. hexadecane):[34]

$$D(F) = L_T \coth\left(\frac{Fa}{k_BT} - \frac{k_BT}{Fa}\right) \qquad (6)$$

where $L_T = L_{contour} + n_{FJC}/k_s$ is the total contour length of the bridging chain which takes into account extensibility of the statistical segments, k_s = 150 N/m is the statistical segment elasticity, n_{FJC} is the number of statistical segments, *a* is the statistical segment length which was fixed to its known value of 0.7 nm, T is the absolute temperature, and k_B is Boltzmann's constant. These data were also plotted against a Markovian two-level thermodynamic model[95] (Figure 7B, red dashed line), using the parameters which are known to describe well the extensional behavior of PEO in PBS solution with a bare Si_3N_4 probe tip.[34] This model takes into account both entropic and enthalpic contributions to elastic deformation, and it has been suggested that the additional force required to extend PEO in aqueous solution (relative to nonpolar solvents) is due to the presence of a fully reversible, strain-induced conformational transition from the water-bound, contracted trans-trans-gauche (ttg) state to the more extended trans-trans-trans (ttt) state:

(93) Ortiz, C.; Hadziiouannou, G. *Macromolecules* **1999**, *32*, 780–787.
(94) Marko, J. F.; Siggia, E. D. *Macromolecules* **1995**, *28*, 8759.
(95) Rief, M.; Fernandez, J. M.; Gaub, H. E. *Phys. Rev. Lett.* **1998**, *81*, 4764–4767.

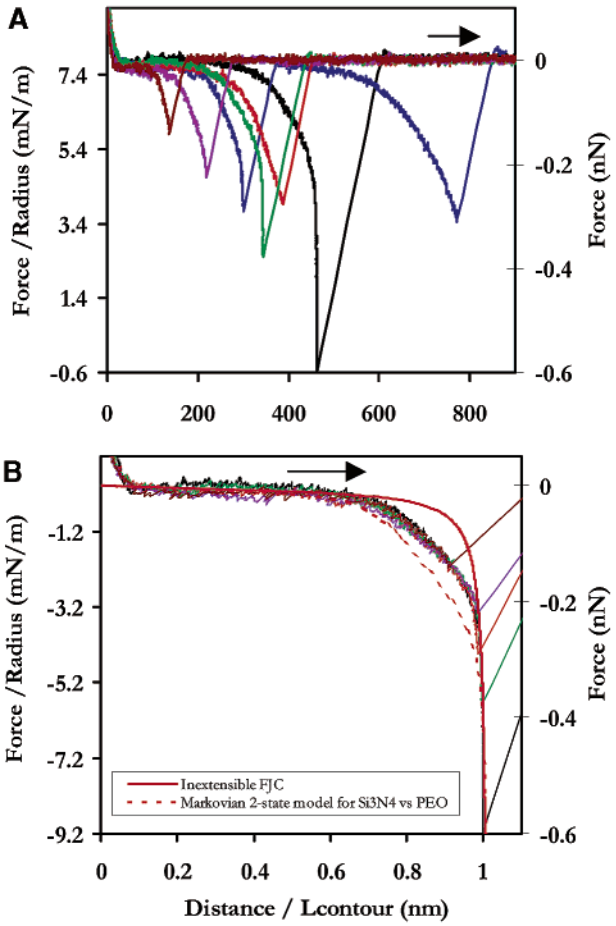

Figure 7. (A) Individual overlaid retraction curves of an HSA-grafted probe tip from a PEO_{50K}−Au substrate, showing extension of individual polymer chains. (B) The overlaid curves in (A) have been normalized by $L_{contour}$ of each bridging chain segment to yield a master curve which represents the molecular elasticity of the bridging chain macromolecule. The master curve is compared with the inextensible freely jointed chain model[124] (solid red line) and the Markovian two-level model[34] (dashed red line) known to represent the extension of PEO in aqueous solution. The model parameters employed were as follows: $\Delta G = 3 \pm 0.3\ k_BT$, $l_u = 0.358$ nm, $l_f = 0.28 \pm 0.005$ nm, $a \sim 2l_u = 0.7$ nm, $k_s = 150$ N/m.

$$D(F) = n_{Mar}\left(\frac{l_u}{e^{-\Delta G/k_BT}+1} + \frac{l_f}{e^{-\Delta G/k_BT}+1}\right)\left[\coth\left(\frac{Fa}{k_BT}\right) - \frac{k_BT}{Fa}\right] + n_{Mar}\frac{F}{k_s} \quad (7)$$

where l_f is the length of the contracted polymer subunit (for ttg, $l_f = 0.278$ nm), l_u is the length of the extended polymer subunit (for ttt, $l_u = 0.358$ nm), n_{Mar} is the number of extended segments (ttt), $\Delta G = 3 \pm 0.3\ k_BT$ is the Gibbs free energy difference between the ttg and ttt conformation, $a = 0.7$ nm is the statistical segment length, and $k_s = 150$ N/m is the segment elasticity.[34] The experimental data corresponding to these theoretical models, previously reported by Oesterhelt et al.,[34] were also reproduced in our laboratory (data not shown). Surprisingly, it is noted that in the experiments performed here with an HSA-grafted probe tip, the magnitude of the restoring force is shifted to slightly lower values in the intermediate strain regime (relative to that performed with a bare Si_3N_4 probe tip) and can possibly be attributed to either distortion of the local water structure around the PEO in the vicinity of the probe tip or a restriction of the hydrogen bonding capability of PEO due to the competitive water bonding of the approaching HSA molecules.

Table 3

total dataset including nonadhesion (n = 324,[a] 100% of total)	
$\langle F_{adh}\rangle$ (nN)	0.05 ± 0.09
$\langle F_{adh}\rangle/R_{tip}$ (mN/m)	0.73 ± 1.5
$\langle D_{adh}\rangle$ (nm)	104.7 ± 119.5
long-range chain-pulling adhesive events including weak adhesion (n = 257,[a] 79% of total)	
$\langle F_{adh}\rangle$ (nN)	0.06 ± 0.10
$\langle F_{adh}\rangle/R_{tip}$ (mN/m)	0.90 ± 1.6
$\langle D_{adh}\rangle$ (nm)	131.9 ± 120.1
$\langle U_d\rangle$ (J)	1.2×10^{-18}
$\langle U_d\rangle$ (k_BT)	296
surface adhesion (n = 3,[a] 1% of total)	
$\langle F_{adh}\rangle$ (nN)	0.11 ± 0.03
$\langle F_{adh}\rangle/R_{tip}$ (mN/m)	1.7 ± 0.4
$\langle D_{adh}\rangle$ (nm)	0.7 ± 1.2
nonadhesion (n = 64,[a] 20% of total)	

[a] n = number of datapoints.

HSA−PEO Adhesion (Table 3). The adhesive or binding force between the HSA probe tip and a PEO chain corresponding to curves of the type obtained in Figure 6B−D (79% of the total dataset) was found to be $\langle F_{adh}\rangle = 0.06 \pm 0.1$ nN, or $\langle F_{adh}\rangle/R_{tip} = 0.9 \pm 1.6$ mN/m, corresponding to a distance of $\langle D_{adh}\rangle = 131.9 \pm 120.1$ nm. For data which exhibited weak adhesion (Figure 6D), F_{adh} was recorded as the maximum adhesive force observed on retraction and D_{adh} was recorded as the distance corresponding to F_{adh}. This dataset clearly demonstrates the formation of attractive contacts between the HSA and PEO, presumably due to hydrogen bonds between protonated basic groups of the HSA and the −O− groups of the PEO, as well as van der Waals and hydrophobic interactions. Since F_{adh} was found to always be less than the predicted force necessary to cleave the weakest covalent bond (i.e., the Au−S bond; $F_{cleavage} \approx 2-3$ nN[93]), it is assured that the PEO chain always detaches from the probe tip after each force spectroscopy experiment. For these experiments, the adhesion energy per unit area, $\langle W_{exp}\rangle$, was not calculated from the $\langle F_{adh}\rangle$ value using contact mechanical theories[96−98] because the hemispherical geometry does not hold for a single macromolecule desorbing from a hemispherical probe tip. The energy dissipated during the loading−unloading cycle, U_d, was determined by the molecular elasticity of the bridging chain segment and the desorption or detachment of the PEO chain segments from the HSA probe tip. The molecular elasticity contribution can be obtained via integration of eq 7 and will be a function of the bridging chain segment detachment or desorption force, F_{adh}, and the corresponding detachment distance, D_{adh}. Incorporating all adhesion events from force curves of the types shown in Figure 6B−D, $\langle U_d\rangle$ (molecular elasticity) was calculated to be 1.2×10^{-18} J = 296 k_BT.

Statistical Analysis of Adhesion Forces and Distances. Figure 8A plots the values of F_{adh}/R_{tip} (mN/m) versus D_{adh} (nm) for individual HRFS experiments on retraction for the HSA probe tip versus the PEO−Au surfaces in PBS for the entire dataset, including nonadhesion values (black diamond symbols), compared to bare

(96) Burnham, N. A.; Colton, R. J. In *Scanning Tunneling Microscopy and Spectroscopy: Theory, Techniques, and Applications*; Bonnel, D. A., Ed.; VCH Publishers: New York, 1993; pp 191−249.
(97) Johnson, K. L.; Kendall, K.; Roberts, A. D. *Proc. R. Soc. London* **1971**, *A324*, 301−313.
(98) Derjaguin, B. V.; Muller, V. M.; Toporov, Y. P. *J. Colloid Interface Sci.* **1975**, *53*, 314−326.

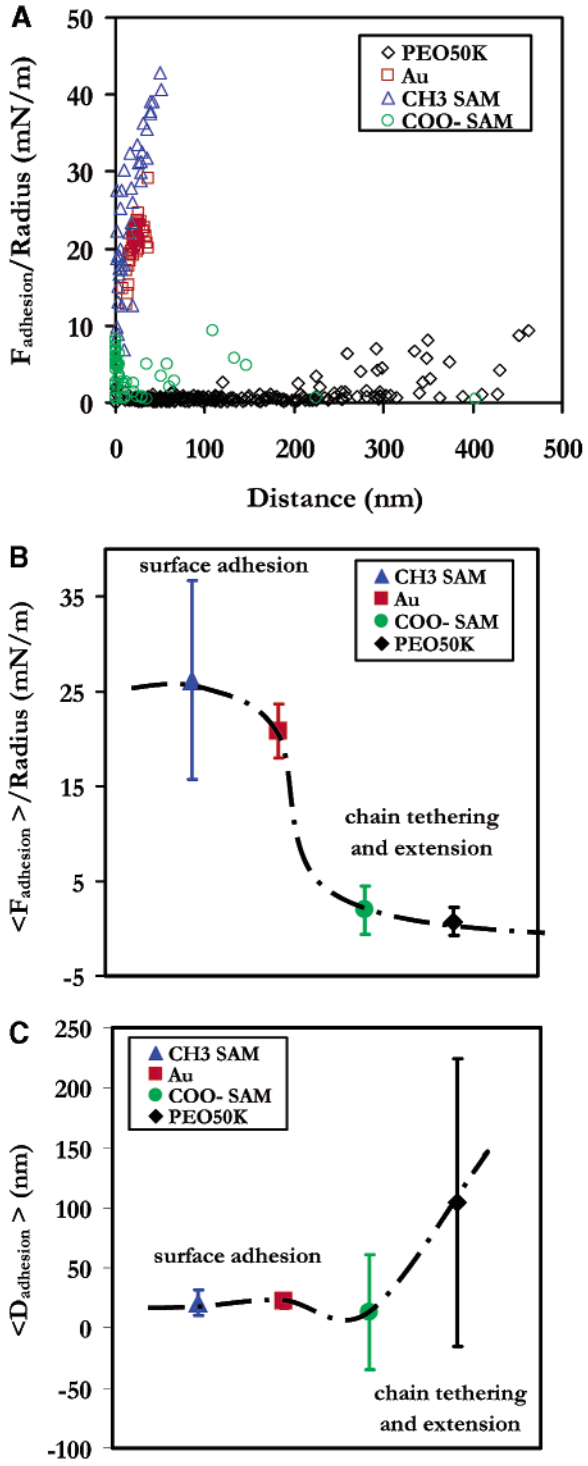

Figure 8. (A) Experimentally observed adhesion forces and distances taken from the minima in attractive peaks from individual Force (nN) (linear scale) versus Distance (nm) retraction curves, (B) average forces of adhesion shown with standard deviations (the dashed line is included to guide the eye), and (C) average distances of adhesion shown with standard deviations (the dashed line is included to guide the eye) of an HSA-grafted probe tip on Au (red squares), a CH_3-terminated SAM (blue triangles), a COO^--terminated SAM (green circles), and PEO_{50K}−Au (black diamonds).

Au (red square symbols), as well as CH_3- and COO^--terminated SAM substrates (blue triangle and green circle symbols, respectively) reported previously.[58] Figure 8B,C plots the mean and standard deviation values $\langle F_{adh}\rangle/R_{tip}$ (mN/m) and $\langle D_{adh}\rangle$ (nm), respectively, and Figure 9 gives the adhesion probability distribution histograms corresponding to these data for PEO shown in Figure 8A. For the entire PEO dataset, $\langle F_{adh}\rangle = 0.05 \pm 0.09$ nN or $\langle F_{adh}\rangle/R_{tip} = 0.73 \pm 1.5$ mN/m, corresponding to a distance of $\langle D_{adh}\rangle = 104.7 \pm 119.5$ nm which is ∼97% less than that for the CH_3-terminated SAM and Au surfaces and ∼62% less than that for the COO^--terminated SAM surface.[58] As mentioned previously, short-range surface adhesion is eliminated on the PEO−Au surface. The broad distribution and large standard deviation of $\langle D_{adh}\rangle$ on the Au−PEO surface reflect the nonspecificity of the PEO chain segment physisorption to the HSA probe tip, which causes the PEO chain to adsorb various amounts of chain segments to the probe tip, as well as polydispersity of the polymer chains. Hence, as the adhesion mechanism varies from short-range surface adhesion to chain tethering and long-range chain extension, a drop in the adhesive force is observed, as well as a broadening of the adhesion distance distribution (Figure 9).

Frequency of Adhesion. Figure 10A compares the frequency of the observed total adhesion events (i.e., the percentage of the total number of force curves for which either surface adhesion or chain tethering and extension was observed) for HSA versus PEO−Au (black diamond) with that of Au (red square), as well as those of the CH_3- and COO^--terminated SAM substrates (blue triangle and green circle, respectively). These data are broken down into the two specific mechanisms of adhesion in Figure 10B which compares the frequencies of protein or polymer extension events and Figure 10C which compares the frequencies of surface adhesion events. The effectiveness of PEO_{50K} on reducing adhesive events is strikingly obvious from Figure 10A when compared to the hydrophobic Au and CH_3-terminated SAM surfaces. Figure 10B should be read with care, since most likely protein unfolding and extension are taking place on the CH_3-terminated SAM, COO^--terminated SAM, and Au surfaces but cannot be detected because of the large cantilever instability regime that exists on retraction for high adhesive forces. This would cause the percentages of protein extension to be underestimated. Additionally, the percentage of extension on the PEO substrate is naturally higher, since there is the possibility of both protein *and* polymer extension.

Discussion

Prior work related to this study reported in the literature includes the measurement of forces between surfaces bearing adsorbed PEO layers using the SFA[99−105] and the AFM,[106] electrostatically anchored PEO brushes using the AFM[107] and the SFA,[20] and weakly overlapping, end-grafted, low molecular weight (2K) PEG brushes using the AFM.[108] A few force spectroscopy studies have been reported involving HSA with the AFM[109−111] and the SFA.[112,113] The only reports, to our knowledge, on the direct measurement of protein−PEO interactions include studies between streptavidin and electrostatically anchored lipid bilayers displaying lower molecular weight (1.2K−5K) PEG chains in both the mushroom and brush regimes, using the SFA.[17,65] In this study, a combined theoretical and experimental approach was employed to study the molecular origins of PEO hemocompatibility and yielded significant information on this technologically important higher molecular weight regime using a well-characterized, chemically end-grafted system. Two critical components of this work were a detailed comparison of the experimental results to (1) HRFS experiments on Au (the "background" substrate for the PEO) and (2) quantitative

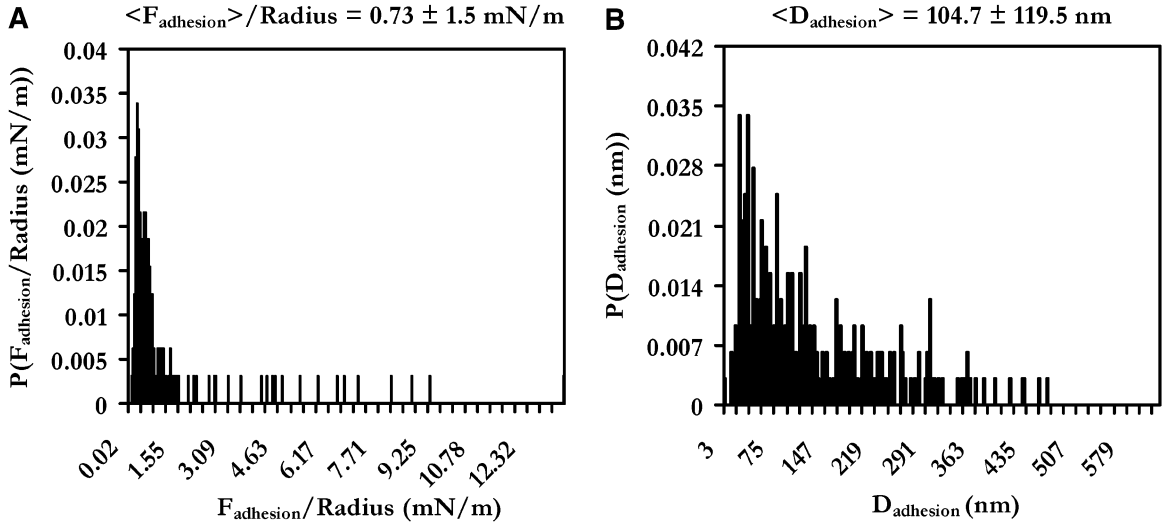

Figure 9. Probability distribution histograms corresponding to the experimentally observed adhesion forces (A) and distances (B) shown in Figure 8A for the HSA-grafted probe tip versus PEO50K-Au substratein PBS solution.

predictions of various theories calculated based on known parameters.

Experimental Data on Approach. It was found that the HSA versus PEO interaction (Figure 5) exhibits a rather broad, nonhysteretic, nonlinear, purely repulsive net force beginning at D < 30 nm. The relatively low standard deviation indicates that this interaction was fairly uniform both at different locations on the sample surface and for repeated HRFS experiments at a single location. It is clear from these data that under these conditions and at long distances, the repulsive force constituents outweigh any attractive hydrophobic and van der Waals interactions. A comparison to the predicted theoretical force constituents including the electrostatic double layer repulsion (based on the Poisson−Boltzmann theory), steric repulsion (based on the Dolan−Edwards theory for configurational entropy), and attractive van der Waals forces (based on Lifshitz theory) is enlightening. Although it is reasonable to assume that steric forces may be present at separation distances equal to a few multiples of $\langle R_F \rangle$ since the chain will statistically explore more extended configurations beyond $\langle R_F \rangle$, the magnitude of the experimentally measured force is severely underestimated by any of the individual theoretical predictions, or a linear summation thereof. This additional repulsive force is most likely one of the key factors in understanding the protein-resistant properties of PEO. As discussed in the Appendix, it is worthwhile to note, based on our AFM imaging studies of PEO and previous studies on end-grafted polymer systems,[70] that for such low-density PEO mushrooms in this molecular weight range the incompressible layer thickness of the PEO, $D_{PEO(final)}$, and hence the offset of the D = 0 position, is expected to be negligible because the polymer chain compression is not highly restricted by excluded volume of neighboring chains. Even if this was not the case, the data would be shifted by $D_{PEO(final)}$ along the distance (x) axis to the right, thus increasing the range of the interaction, and hence this general conclusion would be still be valid and, in fact, even more pronounced. The contribution of compressional deformation of the HSA (e.g., from conformational transitions, mechanical denaturation, etc.) on the probe tip to this net force has been ruled out via control experiments with both Si_3N_4 and glutaraldehyde probe tips on similar end-grafted PEO_{50K} mushroom surfaces, which show a similar range and magnitude of the net repulsive force on approach (data not shown), as well as by estimations of the compressive force per protein which is much less than the expected forces needed for significant distortions of the protein structure (see Appendix).

Feldman et al.[108] have reported ionic strength dependent, long-range (D < 50 nm), nonlinear repulsive forces on a short methoxy-oligo(ethylene glycol) (OEG) terminated SAM on Au using the AFM (which has no steric interactions since these are solely associated with long polymer chains), and interpreted this force as originating from electrostatic double layer repulsion due to an effective surface charge imparted by a polarizable dipole layer on the surface. Additional resistance of a stable, long-range oriented water interphase layer templated by the ordered structure of the OEG SAM on Au is also possible. Even though HSA is known to have a 0.55 nm thick monolayer of closely associated water molecules on its surface[92] and additional translationally restricted interfacial water layers may exist, this latter mechanism seems unlikely in the PEO_{50K} system studied here, given the long range of the interaction observed, and the high macromolecular flexibility and mobility of the PEO chain. One possible explanation for this additional repulsive force, which is also supported by single molecule extensional experiments discussed in the following section, is enthalpic disruption

(99) Israelachvili, J. N.; Tandon, R. K.; White, L. R. *J. Colloid Interface Sci.* **1980**, *78*, 430−443.
(100) Klein, J.; Luckham, P. *Nature* **1982**, *300*, 429−431.
(101) Klein, J.; Luckham, P. *Nature* **1984**, *308*, 836−837.
(102) Klein, J.; Luckham, P. *Macromolecules* **1984**, *17*, 1041−1048.
(103) Kuhl, T.; Guo, Y.; Alderfer, J. L.; Berman, A. D.; Leckband, D.; Israelachvili, J. N.; Hui, S. W. *Langmuir* **1996**, *12*, 3003−3014.
(104) Kuhl, T. L.; Berman, A. D.; Hui, S. W.; Israelachvili, J. N. *Macromolecules* **1998**, *31*, 8250−8257.
(105) Hui, S. W.; Kuhl, T. L.; Guo, Y. Q.; Israelachvili, J. N. *Colloids Surf., B* **1999**, *14*, 213−222.
(106) Braithwaite, G. J. C.; Howe, A.; Luckham, P. F. *Langmuir* **1996**, *12*, 4224−4237.
(107) Butt, H. J.; Kappl, M.; Mueller, H.; Raiteri, R.; Meyer, W.; Rühe, J. *Langmuir* **1999**, *15*, 2559−2565.
(108) Feldman, K.; Haehner, G.; Spenser, N. D.; Harder, P.; Grunze, M. *J. Am. Chem. Soc.* **1999**, *121*, 10134−10141.
(109) Kidoaki, S.; Matsuda, T. *Langmuir* **1999**, *15*, 7639.
(110) Kidoaki, S.; Nakayama, Y.; Takehisa, M. *Langmuir* **2001**, *17*, 1080−1087.
(111) Vansteenkiste, S. O.; Corneillie, S. I.; Schacht, E. H.; Chen, X.; Davies, M. C.; Moens, M.; Van Vaeck, L. *Langmuir* **2000**, *16*, 3330.
(112) Claesson, P. M.; Blomberg, E.; Froberg, J. C.; Nylander, T.; Arnebrant, T. *Adv. Colloid Interface Sci.* **1995**, *57*, 161−227.
(113) Blomberg, E.; Claesson, P. M.; Tilton, R. D. *J. Colloid Interface Sci.* **1994**, *166*, 427.

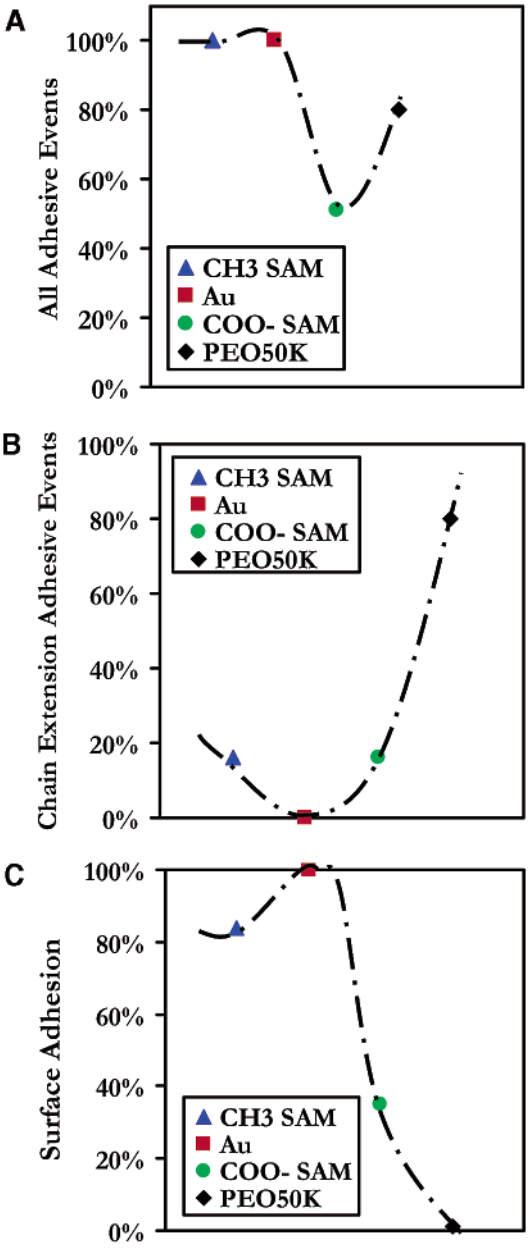

Figure 10. Percentage of the number of force curves in a given dataset which exhibited (A) any adhesive event (e.g., surface adhesion, and/or protein/PEO chain tethering and extension), (B) only protein/PEO extension, and (C) only surface adhesion for an HSA probe tip on Au (red squares), a CH_3-terminated hydrocarbon SAM (blue triangles), a COO^--terminated hydrocarbon SAM (green circles), and PEO_{50K}—Au (black diamonds).

of the compacted, water-bound ttg helical supramolecular structure of the PEO chain under compression to the extended ttt state; that is, the polymer chain extends in the *x*/*y* plane of the sample perpendicular to the direction of the applied compressive force (*z*).

As mentioned previously, an interesting local maximum followed by a drop in the net repulsive force with decreasing separation distance was observed at D < 4 nm when the protein probe tip was pushed into close contact with the PEO. The source of this local maximum may be one or a combination of the following: (1) penetration of the probe tip apex through the polymer layer so that it may form attractive interactions (e.g., van der Waals) with the underlying Au surface, (2) additional attractive interactions, such as hydrogen bonding, between the HSA and PEO, (3) rearrangement of hydration layers, and (4) polymer conformational transitions upon compression such as "escape transitions".[47]

Table 4

symbol	definition	numerical value (s)	reference
t_{HOH}	time between successive Brownian collisions of a water molecule with its neighbors	10^{-12}	
t_{amino}(HSA)	time scale for reorientation of amino acid side chains in HSA	10^{-10}–10^{-11}	123
τ_R(HSA)	time scale for rotation of HSA	10^{-8}–10^{-9}	92
$\tau_{Zimm}(PEO_{50K})$	Zimm time (PEO_{50K})	10^{-7}	115
$\tau_{Rouse}(PEO_{50K})$	Rouse time (PEO_{50K})	10^{-5}	111
t_c	time scale for thermal oscillations of cantilever = inverse resonant frequency (ω^{-1}) in water	10^{-3}	measured
t_L(HSA)	time scale for ligand binding to HSA	10^{-2}	92
t_{exp}	total HRFS experimental time	10^{0}	set

Experimental Data on Retract. Near-complete elimination of surface adhesion was observed on the PEO-grafted surface, relative to the Au and CH_3 surfaces, as evidenced by the nonhysteretic nature of the net repulsive force for D < 30 nm. It is interesting that this result is obtained, considering the very low grafting density and intermediate molecular weight range of the PEO. In 78% of the total HRFS experiments, a number of PEO chain segments become physically adsorbed to the HSA probe tip on approach; this physisorption is strong enough to act as a "tether" and enable extension of individual PEO chains between the surface and probe tip on retract, resulting in a long-range, nonlinear adhesive interaction between the probe tip and surface. Extensive discussion of single molecule force spectroscopy (SMFS) data analysis and comparison with theory (e.g., freely jointed chain, wormlike chain, Markovian two-state model, etc.) has been published previously by us and others[34,93] and will not be repeated here. It is instructive, though, to consider the relevant time scales of various processes involved in particular for these experiments, which are summarized in Table 4. The intrinsic relaxation of a single polymer chain in dilute solution using the classic Rouse approximation of a solvent "draining" freely jointed chain[114] can be described by a characteristic time, τ_{Rouse}, determined by diffusion of segments over the scale of the chain length, $L_{contour}$, giving:

$$\tau_{Rouse} \approx \frac{\eta_{HOH} L_{contour}^2 a}{k_B T} \approx 2.7 \times 10^{-5}\ \text{s}\ (PEO_{50K}) \qquad (8)$$

where η_{HOH} is the viscosity of the solvent (HOH) and $\eta_{HOH}/k_BT = 2.45 \times 10^{-10}$ s·nm^{-3}. The characteristic time for a single polymer chain using the "non-free-draining" Zimm approximation, τ_{Zimm}, is given by:[115]

$$\tau_{Zimm} \approx \frac{\eta_{HOH} R_F^3}{k_B T} \approx 1.6 \times 10^{-7}\text{s}\ (PEO_{50K}) \qquad (9)$$

which includes hydrodynamic effects of trapped solvent

(114) Doi, M.; Edwards, S. F. *The Theory of Polymer Dynamics*; Clarendon Press: Oxford, 1986.

inside the coil. It has been postulated that as a polymer chain is extended it goes from a non-free-draining to a free-draining state because of an increase in the friction coefficient of the polymer chain.[116,117] For either case (free-draining or non-free-draining), since the rate of thermal randomization ($1/\tau_{Rouse} = 3.7 \times 10^4\ s^{-1}$ or $1/\tau_{Zimm} = 6.3 \times 10^6\ s^{-1}$) is much faster than the experimental polymer extension rate ($\approx 1\ s^{-1}$), the polymer configurations are sufficiently randomized by thermal excitations and the polymer extension may thus be treated as quasielastic.[118] As discovered previously,[34] additional force is needed in the extension of individual PEO molecules in aqueous solution (compared to nonpolar solvents) presumably due to enthalpic disruption of the compacted, water-bound ttg helical supramolecular structure as the polymer is extended to the ttt configuration. Surprisingly, in the experiments performed here with an HSA probe tip, the magnitude of the restoring force is shifted to slightly lower values in the intermediate strain regime (relative to that performed with a bare Si_3N_4 probe tip), and can possibly be attributed to distortion of the local water structure around the PEO in the vicinity of the probe tip.

The HSA versus PEO HRFS experiments discussed above clearly demonstrate that, given enough compressive force and time, short-range attractive interactions between the PEO chain segments and the HSA protein surface are formed where the binding force per PEO chain is $\langle F_{adh} \rangle = 0.06 \pm 0.1$ nN and $\langle F_{adh} \rangle / R_{tip} = 0.9 \pm 1.6$ mN/m. The number of proteins involved in this adhesion is unknown but should be less than or equal to the total number of proteins (~134−220) present in the maximum surface interaction area at D = 0. The attractive PEO−HSA binding leads to energy dissipation as the bridging polymer chain stretches and detaches from the probe tip, and the magnitude of this energy dissipation is determined by the area under the molecular elasticity profile of the bridging polymer chain, as well as the binding strength. The presence of attractive interactions and the magnitude of the adhesion energies between HSA and PEO are consistent with the reports on adhesion between streptavidin and electrostatically anchored lipid bilayers reported previously.[17,65] This interaction may have contributions from hydrogen bonds between protonated basic groups of the HSA and the −O− groups of the PEO, and from van der Waals and hydrophobic forces. To deconvolute the constituent contributions to the total net attractive HSA versus PEO binding force, further studies are underway employing "antihydrophobic" agents in the solution, such as 2-propanol, which are substances that increase the water solubility of nonpolar molecules by acting as a bridge between the polar water and nonpolar solute, but do not affect H-bonding strength between solvated molecules.[69,119] Another experiment underway is to employ *lipid-free* HSA, which has exposed hydrophobic channels, to study the effect of lipid complexation on the adhesive binding force.

Conclusions

The net nanoscale force versus separation distance between an HSA-modified probe tip and a surface of neutral, chemically end-grafted PEO_{50K} mushrooms was measured directly on approach (loading) and retract (unloading) in aqueous buffer solution (IS = 0.01 M, pH = 7.4) using the technique of HRFS. On approach, a fairly broad, nonhysteretic, nonlinear, purely repulsive net force is observed to begin at D < 30 nm. The magnitude of this force, even under such low grafting density conditions, is much larger than that predicted by either electrostatic or steric (configurational entropy) theories and is one of the key factors in understanding the protein-resistant properties of PEO. One possible source for this "additional" force, which is also supported by single molecule extensional experiments, is enthalpic disruption of the compacted, water-bound ttg segments and helical supramolecular structure of the PEO chain under compression to the extended ttt state as the chain extends in the *x*/*y* plane of the sample perpendicular to the direction of the applied compressive force (*z*). A local maximum followed by an interesting drop in the net repulsive force with decreasing separation distance is observed at D < 4 nm. During approach of the HSA probe tip on the PEO surface, a number of PEO chain segments become physically adsorbed to the HSA probe tip, enough so that they are strong enough to act as a tether and enable extension of *individual* PEO chains between the surface and probe tip on retract, resulting in a long-range, nonlinear, adhesive interaction between the probe tip and surface. This clearly demonstrates that given enough compressive force and time, short-range attractive interactions between the PEO chain segments and the HSA protein surface may form, where the binding force per PEO chain is $\langle F_{adh} \rangle / R_{tip} = 0.9 \pm 1.6$ mN/m. This interaction may have contributions from hydrogen bonds between protonated basic groups of the HSA and the −O− groups of the PEO and from van der Waals and hydrophobic forces. To deconvolute the constituent contributions to the total net attractive HSA versus PEO binding force, further studies are underway employing antihydrophobic agents and lipid-free HSA to minimize the hydrophobic component of the interaction. In short, we have shown that high-resolution force spectroscopy is a valuable tool to assess biocompatibility at the nanoscale and, combined with theoretical approaches, can provide important information that may be used as a guideline for the design of improved synthetic macromolecular systems for future biomedical applications.

Acknowledgment. The authors thank Professors Paul Laibinis and Michael Rubner of MIT for the use of vital surface preparation and characterization equipment. This research was funded by a National Science Foundation Graduate Fellowship and a Whitaker Foundation Graduate Fellowship.

Appendix

Definition of Distances in HRFS Experiments. Figure 11 is a schematic of all of the distances in the HSA-grafted probe tip versus PEO surface HRFS experiments. The distance of relevance, D, is the separation distance between the gold substrate (or the real D = 0 point) and the surface of the HSA on the probe tip, which equals the height of the PEO chain under compression when in contact, D_{PEO}. D can be defined as follows:

$$D = D_{measured} - D_{HSA(initial)} + D_{PEO(final)} + D_{HSA(final)} \quad \text{(A1)}$$

where $D_{measured}$ is the measured distance from the "apparent" D = 0 to the probe tip, $D_{HSA(initial)}$ is the height of HSA protein at a given separation distance, $D_{HSA(final)}$ is the incompressible height of an HSA protein, and

(115) Zimm, B. H. *J. Chem. Phys.* **1956**, *24*, 269.
(116) deGennes, P. G. *J. Chem. Phys.* **1974**, *60*, 5030.
(117) Pincus, P. *Macromolecules* **1990**, *9*, 386.
(118) Ritchie, K.; Evans, E. *Biophys. J.* **1999**, *76*, 2439−2447.
(119) Craighead, H. G.; Turner, S. W.; Davis, R. C.; James, C.; Perez, A. M.; St. John, P. M.; S., I. M.; Kam, L. S. W.; Turner, J. N.; Banker, G. *Biomed. Microdevices* **1998**, *1*, 49−64.

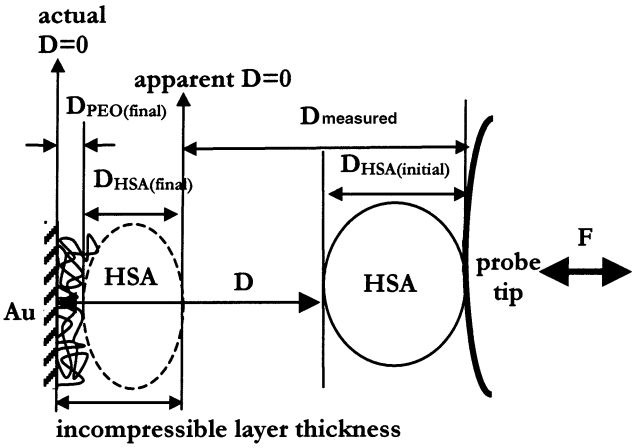

Figure 11. Schematic of the distances in the HSA probe tip versus PEO surface HRFS experients.

$D_{PEO(final)}$ is the incompressible height of the PEO chain. The apparent D = 0 is set as the point where the two respective surfaces have reached their limits of compressibility. This vertical region of apparent infinite slope in the high-force, constant compliance regime is due to the fact that the spring constant of the cantilever is much less than the stiffness of the substrate. For high-density polymer brushes, it has been shown that the height of the incompressible polymer layer, $D_{PEO(final)}$, can be significant.[120,121] However, for low-density PEO mushrooms in the molecular weight range employed here, $D_{PEO(final)}$ is expected to be negligible. In addition, significant distortions (denaturation) of protein structures are expected to take place under ~nN of force.[122−124] The maximum force per protein on approach, F_{max}, at D = 0 was 1.6 pN assuming a triangular shape, or 8.6 pN assuming an ellipsoidal shape lying flat, much less than the expected force needed for HSA denaturation. Hence, it is expected that steric deformations of the protein have negligible contribution to the interaction force profile, that is, $D_{HSA(initial)} = D_{HSA(final)}$. If this is the case, then the last three terms of eq A1 may be neglected and $D \approx D_{measured}$.

Nomenclature

a	polymer statistical segment length for freely jointed chain model (nm)
A	Hamaker constant for van der Waals interaction (J)
A_{132}	Hamaker constant between two macroscopic media 1 and 2 interacting across medium 3 as calculated by Lifshitz theory (J)
A_2	second virial coefficient ($cm^3 \cdot mol/g^2$)
$A_{contact}$	Hertzian elastic contact area between probe tip and surface (nm^2)
$A_{substrate}$	projected maximum interaction area on substrate at D = 0 (nm^2)
A_{tip}	maximum surface interaction area on probe tip at D = 0 (nm^2)
C_M	polymer expansion constant (unitless)
C_∞	polymer characteristic ratio (unitless)
c*	critical overlap concentration of polymer in solution (mol/L)
D	intersurface separation distance (nm)
D_{adh}	distance at which the maximum attractive force measured on retraction takes place (nm)
$D_{measured}$	measured distance from apparent D = 0 to probe tip surface (nm)
$D_{HSA(initial)}$	height of HSA protein layer on probe tip at a given separation distance (nm)
$D_{HSA(final)}$	final, incompressible height of HSA protein layer on probe tip (nm)
D_{max}	maximum distance of interaction on approach (nm)
$D_{PEO(final)}$	final, incompressible height of PEO chain (nm)
F	force between probe tip and surface (nN)
F_{adh}	maximum attractive force measured on retraction (nN)
$F_{cleavage}$	the force necessary to cleave the weakest covalent bond in a molecule (nN)
F_{max}	the maximum compressive force per protein within the maximum probe tip-surface interaction are (nN or pN)
F_{VDW}	intersurface van der Waals force (nN)
h	height of PEO_{50K} chain measured by the AFM (nm)
h	Planck's constant (6.626×10^{-34} J·s)
k_B	Boltzmann's constant (1.38×10^{-23} J/K)
k_c	cantilever spring constant (N/m)
k_s	polymer statistical segment elasticity (N/m)
l	bond length (nm)
$l_{monomer}$	PEO monomer length (nm)
l_u	length of extended polymer subunit in Markovian two-state model (nm)
l_f	length of contracted polymer subunit in Markovian two-state model (nm)
$L_{contour}$	macromolecular extended contour length (nm)
L_T	total contour length of polymer chains for extensible freely jointed chain and Markovian two-state models (nm)
M_n	number-average molecular weight of polymer (g/mol)
M_w	weight-average molecular weight of polymer (g/mol)
n	number of datapoints used in an average or statistical distribution
n_{FJC}, n_{Mar}	number of polymer statistical segments in freely jointed chain model and number of extended (ttt) segments in Markovian two-state model, respectively (unitless)
N	number of repeat units (monomers) in polymer chain (unitless)
N_A	Avogadro's number (6.022×10^{23} mol^{-1})
R	radius of sphere in inverse power law for van der Waals force (nm)
R	universal gas constant (=8.134 J/mol·K)
R_F	Flory radius of polymer chain (nm)
R_{tip}, Radius	probe tip radius measured experimentally by SEM (nm)
R_{hemis}	radius of hemisphere representing probe tip in surface charge model (nm)

(120) Yamamoto, S.; Ejaz, M.; Tsujii, Y.; Fukuda, T. *Macromolecules* **2000**, *33*, 5608−5612.
(121) Yamamoto, S.; Ejaz, M.; Tsujii, Y.; Matsumoto, M.; Fukuda, T. *Macromolecules* **2000**, *33*, 5602−5607.
(122) Rief, M.; Gautel, M.; Oesterhelt, F.; Fernandez, J. M.; Gaub, H. E. *Science* **1997**, *276*, 1109−1112.
(123) Gurd, F. R. N.; Rothgeb, T. M. *Adv. Protein Chem.* **1979**, *33*, 74−165.
(124) Kuhn, W. *Kolloid-Z.* **1934**, *68*, 2.

s	distance between end-grafted polymer chains (nm)
t_{HOH}	time between successive Brownian collisions of a water molecule with its neighbors
t_{amino}(HSA)	time scale for reorientation of amino acid side chains in HSA
t_c	time scale for thermal oscillations of cantilever = inverse resonant frequency (ω^{-1}) in water
t_L(HSA)	time scale for ligand binding to HSA
t_{exp}	total HRFS experimental time
T	absolute temperature (K (Room Temperature = 298))
U_d	energy dissipated during loading/unloading cycle (J)
W_{exp}	experimentally measured adhesion energy per unit area (mJ/m^2)

Greek Symbols

α	Flory polymer chain expansion parameter (unitless)
ϵ	dielectric constant (unitless)
ΔG	Gibbs free energy difference between ttg and ttt conformations (k_BT)
Γ	end-grafted polymer areal chain density (chains/nm^2)
ϕ	volume fraction (unitless)
κ^{-1}	electrostatic interaction Debye length (nm)
η	refractive index (unitless)
η_{HOH}	viscosity of water (g/cm^3)
ρ	density (g/cm^3)
σ	polymer steric parameter (unitless)
σ_{tip}	surface charge/unit area on probe tip in model (C/m^2)
σ_{plane}	surface charge/unit area on substrate in model (C/m^2)
τ_R (HSA)	time scale of rotation of HSA
τ_{Rouse}	Rouse polymer relaxation time (s)
τ_{Zimm}	Zimm polymer relaxation time (s)
Φ	electrical potential (V)
χ	polymer Flory−Huggins interaction parameter (unitless)
ν_e	electronic absorption frequency in UV (s^{-1})

Units

C	coulombs
J	joules
N	newtons
nN	nanonewtons
K	kelvins
m	meters
nm	nanometers
V	volts

Abbreviations

AFM	atomic force microscope
DI	deionized
DLVO	Derjaguin−Landau−Verwey−Overbeek
FJC	freely jointed chain
FW	formula weight
GPC	gel permeation chromatography
HRFS	high-resolution force spectroscopy
HSA	human serum albumin
IS	ionic strength
MFP	molecular force probe
PBS	phosphate-buffered saline
PDI	polydispersity index
PEO	poly(ethylene oxide)
SAM	self-assembled monolayer
SFA	surface force apparatus
SMFS	single molecule force spectroscopy
ttt	trans-trans-trans conformation
ttg	trans-trans-gauche conformation
VDW	van der Waals

LA034057L